universität wien

MASTERARBEIT / MASTER'S THESIS

Titel der Masterarbeit / Title of the Master 's Thesis

„Biogeochemical behaviour of Chromium in rhizosphere systems – from microreactor to paddy soil experiment "

verfasst von / submitted by

Anna Sabrina Kistler, B.Sc.

angestrebter akademischer Grad / in partial fulfilment of the requirements for the degree of

Master of Science (MSc)

Wien, 2024 / Vienna 2024

Studienkennzahl lt. Studienblatt / degree programme code as it appears on the student record sheet:	UA 066 299
Studienrichtung lt. Studienblatt / degree programme as it appears on the student record sheet:	Masterstudium Environmental Science
Betreut von / Supervisor:	Univ.-Prof. Dipl.-Geol. Dr. Stephan M. Kraemer

Abstract

Chromium (Cr), in its hexavalent form, is known to be a toxic heavy metal that poses threats to the environment, especially when considering the widespread use and mining of Cr. High levels of Cr in soils pose severe hazards to plants, animals, and humans, attracting global attention. Complex mechanisms and multiple factors can control the speciation, mobility, and bioavailability of Cr in soil systems. Organic ligands significantly impact the fate and transport of Cr and its solubility; It has been demonstrated that siderophores and organic acids facilitate the dissolution of Cr from hydroxide minerals. Chromium pollution is especially prevalent in the Sukinda Valley in India, where the largest chromite ore reservoir in the country is located. Whilst increased environmental risks are inevitable in this region, not much is known about the intricate interplay between the rice rhizosphere, chromium, and ligands. This study conducted a suite of experiments to provide new insights into the Cr behaviour in contaminated paddy soil. Soil analyses were conducted, followed by a batch soil leaching experiment alongside a rice growth mesocosm experiment. Additionally, an attempt to design a new soil-on-a-chip model was carried out. Soil analyses suggested a very high Cr concentration (~209 mg/kg) in the bulk soil. Batch dissolution results show that siderophore (desferrioxamine B) and organic acids (citric and oxalic acid) can promote Cr dissolution not only from chromium(III) hydroxides but also from soil materials. During the time course of the rice growing experiments, elevated levels of aqueous Cr were detected after the addition of oxalic acids to the system. However, it is difficult to assess what primarily drives the observed results as additional factors (pH, Eh, Fe and Mn) could induce Cr dissolution. It would be valuable for further experiments that determine the relative importance of these factors. Nevertheless, results from this study can provide useful information as to the Cr biogeochemical cycling in a complex system.

Deutsche Kurzzusammenfassung

Chrom (Cr) ist ein giftiges Schwermetall, das aufgrund seiner weit verbreiteten Verwendung und Förderung eine ernsthafte Bedrohung für die Umwelt darstellt. Hohe Cr-Werte im Boden stellen eine Gefahr für Pflanzen, Tiere und Menschen dar und ziehen deswegen weltweit Aufmerksamkeit auf sich. Komplexe Mechanismen und verschiedene Faktoren kontrollieren die Speziation, Mobilität und Bioverfügbarkeit von Cr im Boden. Liganden haben erhebliche Auswirkungen auf die Oxidationsstufe und den Transport von Cr, sowie auf dessen Löslichkeit. Siderophore und organische Säuren haben sich als förderlich für die Auflösung von Chrom aus Hydroxidmineralen erwiesen. Chromverschmutzung ist besonders im Sukinda-Tal in Indien verbreitet, da es das größte Chromerz Reservoir des Landes besitzt. Chromkontamination in Reisfeldern ist in der Region somit unvermeidlich. Es ist jedoch wenig bekannt über das komplexe Zusammenspiel zwischen der Reisrhizosphäre, Chrom und Liganden. In dieser Studie wurden verschiedene Experimente durchgeführt, um neue Einblicke in den kontaminierten Reisboden zu gewinnen. Es wurde eine Bodenanalyse durchgeführt, gefolgt von einem Batch-Experiment, und schließlich wurde ein Topfexperiment durchgeführt. Darüber hinaus wurde ein Versuch unternommen, ein neues „Soil-on-a-chip“ Modell zu entwerfen. In Bezug auf die Bodenanalyse wurde eine klare Cr-Kontamination mit Werten von bis zu 209 mg/kg festgestellt. Die Batch-Ergebnisse zeigen, dass der Siderophor Desferrioxamin B und organische Säuren (Zitronen- und Oxalsäure) die Auflösung von Cr nicht nur aus Chromhydroxid, sondern auch aus Cr-kontaminiertem Boden fördern können. Bei dem Reiswachstumsexperiment wurden erhöhte Cr-Werte in Lösung nach Zugabe von Oxalsäure zum Boden festgestellt. Bei den Ergebnissen des Topfexperiments konnten wir jedoch nicht identifizieren, was die Auflösung antreibt, da es mehrere Faktoren (pH, Eh, Fe und Mn) gab, die die Cr-Auflösung induzieren können. Trotzdem können diese Ergebnisse für weitere Experimente nützlich sein, bei denen die Korrelation jedes Einflussfaktors auf die Cr-Auflösung bestimmt werden sollte.

Table of Contents

List of tables

List of figures

List of pictures

List of equations

Introduction

Chromium in the Environment

Chromium (Cr) pollution is a global issue and a severe threat to the environment and the health of millions of people[1]. It is the 7th most abundant element in the earth´s crust and can be introduced into the environment by anthropogenic emissions or geological processes[2]. The primary sources of geogenic Cr in soil are ophiolite serpentine complexes, ultramafic and basaltic rocks and their weathered products[3]. The natural level of chromium in sedimentary and igneous rocks is usually low (~ 10-120 mg/kg), but it can reach higher concentrations in ultramafic and some basaltic igneous rocks (e.g., 200-3900 mg/kg)[4]. Cr exists in all environmental compartments, including rock, soil, water and air. Generally, in unpolluted soils, Cr is of geogenic origins with a concentration between 10-50mg Cr per kg of dry soil and even lower levels in water and air[5]. On the other hand, Cr is a metal that is industrially used in chemical processing, multiple commercial products such as paints and tannings, and the production of stainless steel and alloys[6]. The demand for Cr is expected to increase owing to the rising production levels of stainless steel related products, such as automotive, aerospace and electronics[7]. Therefore, chromite, the primary ore of the element Cr, has been mined extensively in countries including Kazakhstan, South Africa and India, with a global production of 41 million tons in 2022 alone, according to the U.S. Geological Survey, Mineral Commodity Summary, January 2023[8].

India's largest chromite ore deposit is located in the Sukinda Valley, stretching over 420 km2 and accounting for 97% of India's chromite ore deposits[9]. The mining operations include 20 open cast and two underground mines, resulting in extensive soil contamination due to the generation of 160 million tons of overburden[10]. This area also releases 11.73 tons of hexavalent Cr into the environment annually, making it one of the world's most polluted places [1, 10]. These continuous mining activities have introduced a large amount of Cr into agricultural soils, groundwater and the air.

Biogeochemical Properties of Chromium

Chromium is a transition metal that is redox sensitive. It has a relatively wide range of oxidation states from -2 to +6, but only Cr(III) and Cr(VI) are stable and common oxidation states under most conditions of the Earth's surficial environment[11]. In contrast to many other heavy metals, Cr(III) and Cr(VI) are individually regulated by the Environmental Protection Agency (EPA) as they have different chemical, epidemiological, and toxicological characteristics[12]. As for their sorption and bioavailability in soil, absorption and transport to aerial portions, and toxicity, the two species of Cr differ substantially[13]. Cr(III) is an essential trace element for humans and animals as part of the lipid and sugar metabolism, but it may not be required by plants[13, 14]. On the other hand, Cr(VI) is highly toxic due to its corrosive and strong oxidizing properties to all living organisms. The Agency for Toxic Substances and Disease Registry (ATSDR) ranked hexavalent Cr 17th on their 2022 Substance priority list[15]. It is also categorized as carcinogenic to humans, according to the EPA[16]. The World Health Organisation declared

the drinking water standard for Cr to be below 0.1 mg/l, respectively[17]. Comparing the mobility of the different oxidation states, Cr(III) is chemically immobile as it forms low solubility (oxy)hydroxides and stable surface complexes. In contrast, hexavalent Cr is mobile in most aquatic environments because it is a weakly adsorbing (oxy)anion[14].

The speciation and mobility of Cr is influenced by multiple factors such as pH and the electrical potential (Eh)[14]. Figure 1 shows the different hydrolysis speciation and valence states of Cr over a pH range from acidic to basic conditions and over a span of Eh values that are occurring in nature. This diagram assumes that the condition of the system is a chemical equilibrium. As shown in Figure 1, trivalent Cr is present as cationic species such as Cr^{3+} and Cr hydroxides ($Cr(OH)_3$, $Cr(OH)^{2+}$, $Cr(OH)_2^{+}$), and is mostly stable under relatively reducing conditions (Eh > 100mV)[11]. Cr(III) also displays a low hydroxyl solubility and a strong retention on soil surfaces, limiting its bioavailability and mobility in aqueous systems and soils[18]. Compared to that, Cr (VI) is predicted to be thermodynamically stable in aerobic environments (Eh > ~350 mV) as anionic species such as chromate (CrO_4^{2-}) and protonated chromate ($HCrO_4^{-}$)[14]. In any given environment the redox conditions differ, and Cr can rapidly react with reducing or oxidizing agents present. As the redox state largely determines the toxicity and mobility of Cr, it is essential to understand the influence of redox transformation on the biogeochemical cycling of Cr[19].

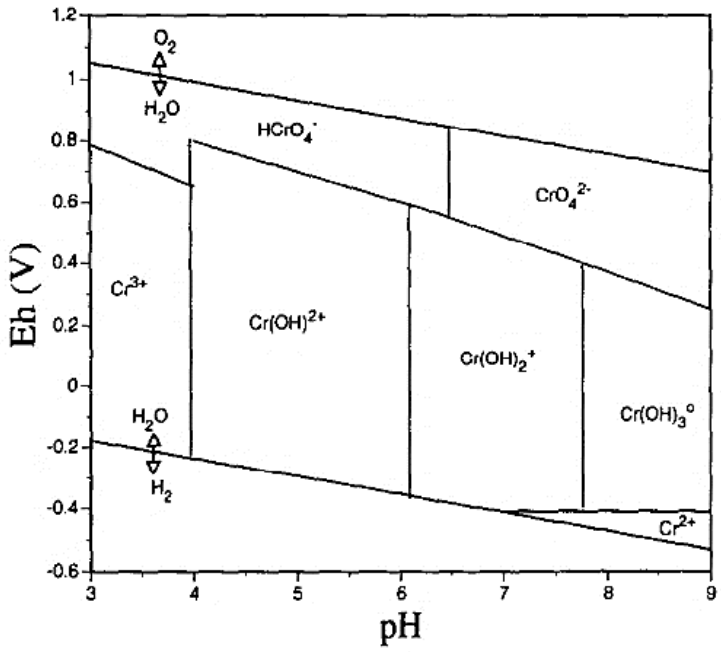

Figure 1. Eh-pH diagram for part of the system Cr-O-OH (Rai et al., 1989)

As the Cr speciation plays a substantial role in its mobility, toxicity, and consequently the remediation strategies for Cr-contaminated soils, obtaining information on the speciation and the factors influencing the Cr speciation[20] is vital. Following a series of efforts by previous studies to characterise the redox transformation in soil systems, mechanisms as to the Cr(III)-Cr(VI) cycles under complicated situations involving both oxidizing and reducing agents[21] are emerging (Figure 2).

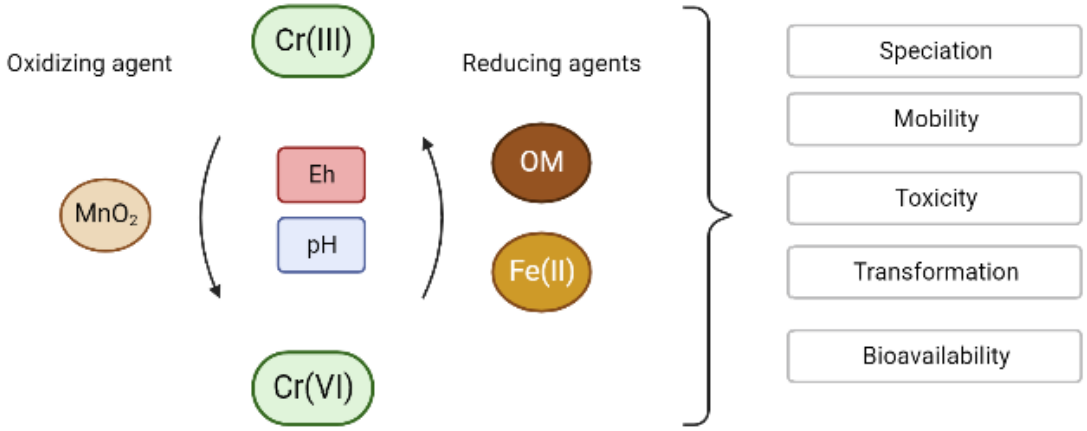

Figure 2. Schematic graph of the Redox cycle of Chromium, including the factors influencing Cr speciation in the environment and the compartments that are affected by the speciation change of Cr (Created with BioRender.com)

Cr(VI) reduction is mediated by various elements present in the environment, such as ferrous iron (Fe), sulphides and organic matter, as shown in Figure 2[11]. One typical example is the reaction of hexavalent Cr with aqueous Fe(II), where Cr(VI) can be reduced to Cr(III) in seconds, forming Fe, $Cr(OH)_3$ solids. This reduction is of environmental benefit as it transforms a hazardous species into a less hazardous one with low mobility, solubility, and toxicity. This solid form of trivalent Cr also has a lower potential to re-oxidize to hexavalent Cr[22]. Another environmentally relevant example of this process is the Cr reduction by organic matter[19]. James and Bartlett [19] found that gallic and ascorbic acids are effective reductants of hexavalent Cr. This process results in the formation of Cr(III) and an organic product, with a high probability of forming soluble Cr(III) complexes. However, these complexes may further complex with manganese oxides, which would lead to the reoxidation of Cr, yielding Cr(VI), which would be unfavourable in the environment[19].

Organic ligands

Another factor that influences the solubility and mobility of Cr are organic chelating agents. A ligand refers to an ion or molecule with a functional group that attaches to a central metal atom to form a coordination complex. One or more of the ligand's electron pairs are donated to the metal to form a bond, often through Lewis bases[23]. There are three types of ligands: monodentate ligands that bind to the center with only one atom, for example chloride ions, bidentate ligands binding to a central metal atom at two points, and polydentate ligands with multiple (>2) atoms used to bond to the central metal atom[24]. Naturally occurring ligands include organic acids like oxalic acid, citric acid, and siderophores like desferrioxamine B (Table 1). Siderophores are chelating agents with a low molecular weight that exhibit a strong affinity towards ferric iron, therefore in environments with limited iron supply, microorganisms produce siderophores to enhance iron uptake[25]. It has recently been recognized that siderophores, a structurally diverse group of biogenic chelating agents linked to the uptake of iron and other nutrient metals, may have more complicated roles in environmental processes than previously

thought. Siderophores bind a wide range of heavy metal ions and have been demonstrated to solubilize, complex, and increase the mobility of several potentially toxic metals even though they have long been thought to be highly selective iron binding agents[26]. Furthermore, those ligands can form complexes with Cr due to the high affinity of trivalent Cr for N, O and S donor atoms[27]. Previous studies also revealed that ligands have the acanhe dissolution of sparingly soluble minerals and, therefore, greatly increase the dissolved concentration of metal ions and the dissolution rates[28,29]. This ligand induced dissolution has also been observed for Cr-hydroxide model compounds[30].

Table 1. Structures of Siderophore DFOB, and the organic acids oxalic acid and citric acid (all images of chemical structures were acquired from PubChem[31])

Type	Species	Structure
Siderophore Hydroxamate	Desferrioxamine B (DFOB)	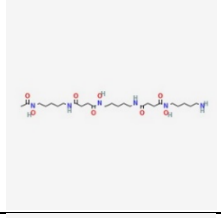
Organic acid	Oxalic acid	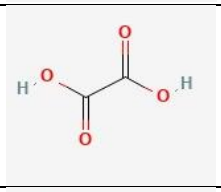
Organic acid	Citric acid	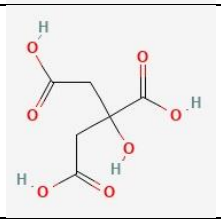

Chromium contamination in soil

Accepting that Cr contamination is a current problem in various countries impacting all compartments (air, water and soil), remediation strategies are a necessity. Several methods to mitigate Cr pollution have been developed. Examples include physical and chemical remediation processes, physiochemical treatment technologies and biological remediation measures[32]. Unfortunately, most remediation processes require a high capital investment, generate large volumes of secondary waste, or are dictated by a vast number of factors influencing treatment efficiency[33]. This, in turn, leads to a continuing and long-lasting issue of Cr pollution that affects all compartments. One compartment that is of particular interest regarding Cr pollution is soil. In general, soils provide numerous ecosystem services to human well-being. They support plant growth and food production, regulate water and nutrient cycles, filter and purify water, store and sequester carbon, and contribute to climate regulation. Understanding soil processes and functions is crucial for sustainable land management, conservation, and maintaining

essential ecosystem services[34]. Chromium ultimately accumulates in crops from contaminated soils, posing severe health concerns to people through contaminated food chains[35]. To understand the implications that Cr contamination of soils can have for humans, it is essential to investigate the speciation, mobility, bioavailability and transportation of Cr in soil-plant systems.

Cr(VI) compounds exhibit a high bioavailability and propensity for transport in water saturated systems whereas Cr(III) compounds can form insoluble chelates or precipitates with low bioavailability and are not easily taken up by plants[21]. No unique mechanism for plant Cr uptake has been discovered because Cr plays no essential part in the metabolism of plants. Although plants are capable of taking up both Cr (III) and Cr (VI), the strategies by which they do so are yet unknown. Plant type and Cr species affect a plant's capacity to absorb Cr[13]. One observed method is that the plants primarily absorb Cr through carriers designed to absorb essential ions for plant metabolism. In the vast majority of plant species, Cr is primarily kept in the root tissues and only moderately translocated to aerial regions. Numerous aspects of plant physiology, including plant type, rate and type of root secretions, root surface area, transpiration, and soil characteristics, including texture, pH, and cation exchange capacity, influence the transfer of Cr between soil and plant[36].

Chromium contaminated paddy field (Sukinda Valley, India)

Considering together all previously discussed sections, I will present results on the Cr-contaminated paddy field in the Sukinda Valley, India. Looking at the region's geology, it becomes apparent that the iron ore group's Archaean low-grade metamorphic rocks, found in the Singhbhum Craton of the Indian Shield, contain the chromite deposits of the Sukinda massifs. This represents the geogenic source of Cr. As the Cr demand increases globally, intensive mining picked up in the region, creating the Sukinda chromite mines[37]. The impact of the anthropogenic Cr source is quite severe for the area, polluting the nearby paddy fields and making it the fourth most polluted area in the world[38]. As rice is considered a staple food, it is of great importance for the region and, therefore, of interest for this study. Additionally, the paddy system is a very complex cosmos because the flooding alters the soil redox states of many elements present[39].

Objective

Extensive research has been conducted on heavy metal redox transformation and cycling in the rhizosphere of a paddy soil-rice system. Previous studies showed that organic acids and siderophores can promote Cr dissolution from hydroxide minerals, which form the foundation of our experiment, but those studies focused on each individual process only in simplified model systems. The present work investigates the biogeochemical behaviour of Cr in the rhizosphere system with a particular focus on the ligand induced Cr dissolution from soil, aiming to piece together the factors that control the Cr cycling.

The goal of this master thesis was to investigate the ligand induced Cr dissolution in a well-controlled paddy system. Soil samples were collected from India and used in the plant mesocosm experiments, with trace metal concentrations and other physico-chemical parameters carefully analysed. To support this, batch leaching experiments with different types of organic ligands were conducted to study the extent and mechanism of Cr dissolution from $Cr(OH)_3$ and the Cr contaminated soil materials. As an extra step, an attempt was made to design a microfluidic device with a reactive surface incorporated.

The research objectives of this thesis were:

- Assessing the influence of ligands, pH, Eh and other factors on Cr biogeochemistry
- Deciphering the multiple processes in the plant-soil system that cause Cr dissolution and, therefore, the environmental risks (from a molecular perspective to a larger scale)
- Developing new systems to study chromium biogeochemistry at the soil pore scale

Materials and Methods

The analyses of bulk soil, and batch dissolution and plant growth experiments were conducted at the Environmental Geochemistry Laboratory within the Centre for Microbiology and Environmental Systems Science (CMESS) at the University of Vienna. The microfluidic reactor experiments were carried out at the Department of Civil and Environmental Engineering of the University of California, Davis.

All solutions were prepared using ultrapure water (resistivity 18.2 MΩcm, MilliQ, Millipore), and all chemicals were of analytical grade. All experiments were conducted using acid cleaned glassware (washed in 5% (v/v) HNO_3).

Paddy soil collection and characterization

The paddy soil samples were collected from the upper layer (0-20 cm) of a Cr-contaminated field in Kaliapani, Sukinda Valley, India (21°03'03.5"N 85°46'16.8"E). The sampling site is approximately 1 km from the active chromite mines (Figure 3).

Figure 3. Location of the sampled paddy field and distance (1 km) to Chromite mine (Google maps. (2023) "Sukinda Valley", Satellite image)

The soil was shipped to the University of Vienna. The soil was completely dry upon arrival, and the sample treatment and characterization were carried out immediately. Firstly, large rocks were sorted out, and the remaining soil was sieved with a 2 mm mesh. To ensure no soil clumps were missed, the rocks

left in the sieve were ground with mortar and pestle and sieved again through a 0.5 mm mesh. This procedure ensured a homogenous soil structure.

Basic soil physiochemical properties were determined using the homogenized soil. The soil pH, measured at a soil to 0.01 M $CaCl_2$ ratio of 1:5 (w/w), was 4.51, and the total organic carbon content of the soil was 1.70 % (measured with a TOC analyzer at the Department of Environmental Geosciences), respectively.

As shown below, two different analyses were conducted to determine the total concentration of metals and relevant elements in soil.

Sequential extraction according to Hasan et al. (2018)

A sequential extraction, according to Hasan et al. (2018) , was conducted with three replicates. The detailed method is described in the following. The metal concentrations for each extraction step were measured by inductively coupled plasma mass spectrometry (ICP-MS 7700, Agilent Technologies, United States) and combined to generate a total concentration of metals in the soil.

Step 1: Targets exchangeable and weak acid soluble metal fractions, including carbonates

40 ml of 0.11 M acetic acid was added to 1g of previously dried soil sample taken in a 50 ml centrifuge tube. This was placed on an overhead shaker (Heidolph Reax 20) for approx. 17 h on medium speed at room temperature. Continuous suspension of the mixture was ensured during shaking. The extract was separated from the solid residue by centrifugation (Eppendorf cold Centrifuge, 5430 R) at 3800 rpm for 20 min. The supernatant was collected in a sterile 50ml tube and further filtered (X500 Minisart HY Syringe filter, 0.45 µm) and acidified (0.2% HNO_3). The pellet was rinsed with 20 ml milliQ water and centrifuged at 3800 rpm for 20 min. The washed supernatant was discarded.

Step 2: Targets reducible fraction of metals in soil

To the residue from the first step, 40 ml of 0.5 M hydroxylamine hydrochloride was added and shaken in an overhead shaker (Heidolph Reax 20) for 17 h at room temperature. The extract was separated from the solid residue by centrifugation and decantation as described in the section Step 1. The pellet was washed with miiliQ water as in the previous step. The supernatant was filtered and acidified as previously described.

Step 3: Targets oxidisable and / or organic bound fraction of metals in soil

Hydrogen peroxide (10 ml, 8.8 M) was added to the washed pellet from step 2 and digested at room temperature for 1h with occasional shaking. The solution was placed into a water bath (SCP Science, DigiREP Jr Digester) at 85°C until the volume was reduced to 1.5 ml. After cooling, additional 10ml Hydrogen peroxide was added to the mixture and again concentrated to 1 ml. It was ensured that the sample did not dry out during the digestion process. To the 1ml solution, 50 ml of 1 M ammonium acetate was added and shaken and extracted as explained above. The residue was washed as explained in the first step.

Step 4: Targets residual or non-silicate bound metal fraction in soil

The residue from step 3 was digested with freshly prepared Aqua Regia (2.3 ml HNO_3 & 7 ml HCl). Firstly, the mixture was standing at room temperature for 16 h to allow slow oxidation of the residue. Following, the mixture was heated up to 80 °C in a water bath (SCP Science, DigiREP Jr Digester) and refluxed for 2 h. After cooling to room temperature, the digest was filtered through a funnel lined with filter paper circles (GE Healthcare Life Sciences Whatman, ashless/Blue ribbon 110mm Diameter). The retained pellet was washed with 0.5 M HNO_3. The filtrated was collected in a 50ml tube and the volume was made up to 50 ml with 0.5 M nitric acid. Blanks were also prepared with each replicate and subjected to the same procedure as that of the samples. Pseudo-total concentration of the metals was calculated from the sum of the four fractions.

Aqua Regia Digest according to the Standard Operating Procedure (SOP)

An Aqua Regia digest, according to the CHEM-LM-SOP-03 (Appendix A), was conducted with three replicates and three blanks to determine the total metal concentration. Into the digestion tubes 0.1 g of previously dried and sieved soil was mixed with 4.5 ml concentrated HCl and 1.5 ml concentrated HNO_3. The digestion was set up for 300 min at a temperature of 80 °C. Following, the solution was transferred into centrifugation tubes and centrifuged at 5000 rpm for 10 min. The supernatant was filtered using 0.45 µm pore size filters.

Quantification of the metals

The supernatants from each step were analysed using inductively coupled plasma optical emission spectroscopy (ICP-OES, CirusCCD, SPECTRO Analytical Instruments GmbH, Germany) and ICP-MS analysis. For ICP-MS, the ICP multi-element standard solution IV (Certipur, Merck, Germany) was used to prepare seven standards ranging from 0.5 to 250 ppb (0.5, 1, 5, 10, 50, 100, and 250 ppb).

The mineral properties of the soil were analysed using X-ray diffraction (XRD) analysis. The soil was ground with mortar and pestle for 15 min to ensure fine grain size. Fine grain size is essential to minimize the micro-absorption corrections, to achieve reproducible peak intensities and to minimize the preferred orientation. The start angle was set to 5°, and the stop angle was 80°. A 2θ step of 0.3°/min was used to reduce interferences resulting from background noise. The XRD analysis has been done with a Benchtop Rigaku MiniFlex 600 diffractometer using a Cu Kα radiation source (λ=1.54Å), with the X-ray tube operating at 20kV and 15mA. The sample analysis and peak matching was performed in the Smart Lab Studio II software (Rigaku), using the COD mineral database.

Batch Experiment Set-up

The rates and extent of Cr dissolution for both Cr hydroxide and the Cr containing soil were conducted as a batch experiment inside a MBraun Labmaster Pro SP anoxic chamber with a N_2 atmosphere using 100 ml Erlenmeyer flasks covered with aluminium foil. The experiment was conducted in duplicate.

The ligands chosen for this study were citric acid, DFOB and oxalic acid, which are of environmental relevance. An electrolyte solution containing 20 mM NaCl was used for both experiments, and the initial pH was 7. The samples taken were filtered and diluted for ICP-MS analysis as described above.

Chromium dissolution rates of model compound Chromium hydroxide

The Cr dissolution rates for $Cr(OH)_3$ were analysed in a batch experiment using 0.2 g/l $Cr(OH)_3$ at a pH of 7 (buffered with HEPES) by adding either 1 mM citric acid or 0.1 mM DFOB. The experiment was conducted over 456 h with five sampling time points (0, 30, 78, 192, and 456 hours). The ingredients were mixed continuously using a magnetic stir bar.

Chromium dissolution rates of Cr-containing soil sample

The Cr dissolution rates for soil samples were analysed in a batch experiment using a 1 g to 100 ml soil-solution ratio. The initial pH of the solutions was adjusted to 7 +/- 0.1, and to each batch, either 0.1 mM DFOB, 1 mM citric acid, or 10 mM oxalic acid were added. The batch analysing the dissolution with DFOB and citric acid was run for 456 h, and the batch analysing dissolution with oxalic acid was run for 142 h. Samples were collected at five time points. The ingredients were mixed continuously using a magnetic stir bar.

Pot Experiment Set-up

The timeline of the entire procedure, including soil analysis, seed germination and planting, addition of ligands and the sample analysis, is shown in Figure 4. The time course ranged from January 2023 to August 2023.

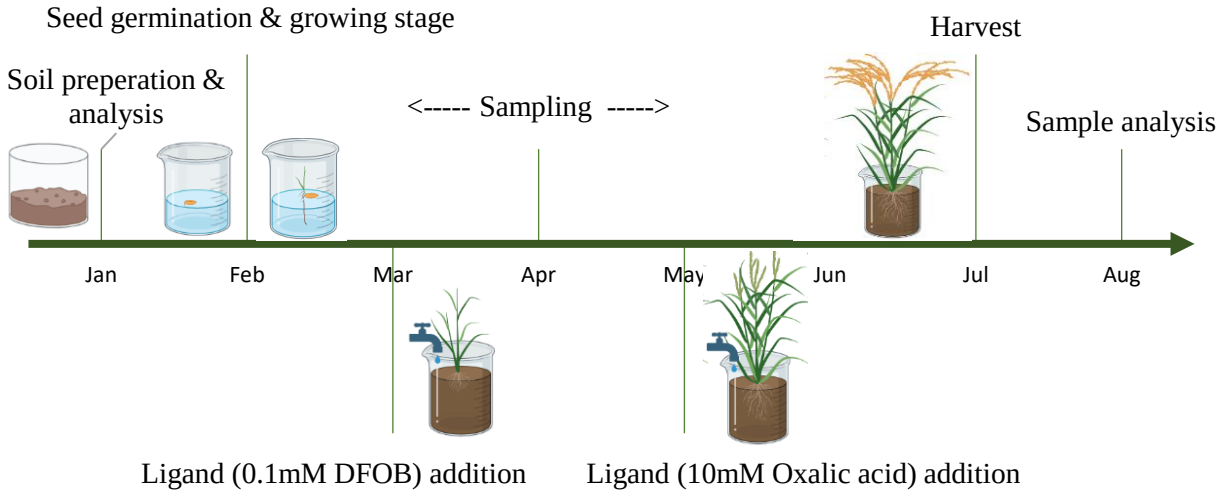

Figure 4. Timeline of the Rice planting, growing and ligand addition experiment over the course of eight months from January-August 2023 (Created with BioRender.com)

Paddy soil treatment

The soil used for the pot experiments was collected from a paddy field in the Sukinda Valley, India (i.e., the same as those utilised in batch experiments) and sieved and homogenised as described above. The soil is thought to have been contaminated with Cr, with total Cr concentrations ranging from 144.1 mg/kg to 209.1 mg/kg. The properties of the paddy soil are summarized in Table 2.

Table 2. Physiochemical properties of the paddy soil before fertilization and planting (n=3).

Parameters	Paddy soil
pH	4.51
Oxygen content	0.23 mg/L (2.4%)
TOC	1.70%
TN	0.25%
Elements	[mg/kg]
Cr	209
Fe	38385
Mn	291
Zn	8663
Exchangeable/weak acid soluble fraction (*Cr*)	2.15
Exchangeable/weak acid soluble fraction (*Fe*)	5500
Reducible fraction (*Cr*)	1.48
Reducible fraction (*Fe*)	3921
Oxidizable fraction (*Cr*)	13.75
Oxidizable fraction (*Fe*)	4629
Residual (*Cr*)	144.2
Residual (*Fe*)	20530

Note: TOC, Total organic carbon; TN, Total nitrogen;

This experiment employed two treatments – one control group and one treatment group. Each group was conducted in triplicates. After the soil had been prepared, 400 g were weight into two-liter glass beakers and 2g of dry pellet fertilizer were added. To ensure a homogenous mixture, 200 ml MilliQ water was added and stirred until the fertilizer was dissolved and distributed evenly. The prepared pots were placed into the climate chamber for seven days to equilibrate.

Rice seed germination

The common rice cultivar *Oryza Sativa japonica* was used in this study. The seeds were germinated according to the "Ronald lab rice growing protocol (February, 2020)" from the University of California Davis (Appendix B) with some modifications. Firstly, the husk was removed from each seed by gently

grinding with a mortar and pestle. Afterwards, they were sterilized with 30% household bleach (DanKlorix containing sodium hypochlorite) for 30 minutes. The treated seeds were rinsed thoroughly with ultra purified water at least three times. Then, they were placed into a 100 ml glass beaker containing ½ Murashige and Skoog Basal medium (MS Media [for 1 liter, 2.2 g MS powder (M5519-10L) and 20 g sucrose was added, adjusted to pH of 5.8 and agar content of 0.8%, autoclaved at 121°C for 15 mins]) and incubated in a climate chamber (Fitotron SGC 120 Biological Chamber, Weiss Technik UK Ltd, United Kingdom) for 7-10 days. The climate chamber was set to 14 h of fluorescent light at 28°C with 75% humidity and 10 h at dark at 26°C with 75% humidity.

Seed planting into Paddy soil

After 7-10 days, the germinated seeds were removed from the growth media, and the roots were carefully rinsed to remove the remaining MS medium. Three holes (0.5 cm diameter) per pot were created using a spatula, and the rice seedlings were transplanted. The roots were gently pressed in the soil and the hole was closed to stabilize the seedling. An irrigation system was implemented to water the pots once a day with a fixed amount of solution to maintain 2 cm water above the soil surface. For the next 45 days, the plants were allowed to grow without interference.

Ligand treatment

After the vegetative growth stage of the rice plants, the treatment group was irrigated using a ligand stock solution (Appendix C). Two ligands, DFOB and oxalic acid, were chosen for this study. Firstly, the rice plants were irrigated 15 ml daily using a 0.1 mM DFOB stock solution (pH 7.5). This treatment was continued for four weeks. Before switching to the second ligand, the plants were watered with tap water for one week to ensure no overlap of the two ligands. Secondly, the plants were irrigated with 30ml per day using a 10 mM oxalic acid stock solution (pH 1.66).

Sampling techniques

The pH and Eh of each rice pot were measured continuously during the experiment using HQ40d Portable Dissolved Oxygen & Conductivity/TDS/Salinity Environmental Monitoring Package (HACH Company, United States). To sample the porewater of the rice plants, Rhizon soil moisture samplers (19.21.22F, Rhizosphere Research Products bv, Netherlands) were employed. The samplers were injected directly into the rice pants' rhizosphere and the bulk soil to compare the different locations. A 3 ml syringe was screwed directly on the lure of the Rhizon sampler. The piston was pulled out completely and secured in place to create a vacuum that drew the porewater into the syringe. The first 5 drops of the collected sample were discarded, and the remaining porewater was filtered with a 0.45 µm filter (Minisart NML hydrophilic 0.45 µm, Sartorius AG, Germany) and further prepared for ICP-MS and Plate reader (Infinite M Plex, Tecan, Switzerland) analysis. After every sample, the Rhizon sampler was washed using a 20% HCl solution and rinsed with MilliQ water.

Sample analysis

The filtered porewater samples were acidified with 1% HNO_3 and diluted to be in the range of 0.5 ppb to 250 ppb to analyse the total element concentration with an ICP-MS. Additionally, the speciation of Fe was conducted according to the ferrozine method protocol (Appendix D) using the Plate reader.

Microfluidic Reactor Fabrication

PDMS reactor mould fabrication protocol

The general fabrication of polydimethylsiloxane (PDMS) microfluidic reactors using soft lithography was conducted as described in Zhu et al. (2022). The moulds were fabricated at the Center for Nano-MicroManufacturing (CNM2) at UC Davis. The first step is developing a mould master, which contains the design of the microfluidic device, which was adapted from a cross-sectional image of sectioned and solidified 3D Ottawa 30-50 sandy soil that was developed by Wang et al. (2018). First, a CAD file of the reactor geometry was made, and a transparency mask from CAD/Art Services, Inc. was printed. Next, a 6" silicon (Si) wafer was prepared by washing it with acetone, isopropanol and DI water and set to dry. A negative photoresist (Kayaku, SU-8 2025) was spin coated onto the wafer and soft baked on a hot plate in order to set the SU-8. The wafer was then loaded into a mask aligner containing the purchased transparency mask, and the wafer was exposed to UV light. This is followed by a post-exposure bake on a hot plate. Finally, the photoresist is being developed using SU-8 developer solution to remove regions that were not cured by the mask aligner and baked again to cure the photoresist fully. To determine the reactor features, the mould was measured with a profilometer. The final mould is an inverse of the reactor geometry, meaning that the grains in the final reactor are holes in the mould. The final dimensions of the reactor are 1 cm x 1.48 cm x 22 µm, where 60% are grains and 40% are accessible pore space, creating a pore volume of 1.3 μm^3 and a total reactor volume of 6.2 μm^3.

PDMS reactor fabrication protocol using soft lithography

The production of microfluidic reactors was conducted after the fabrication of the mould master. A 10:1 mixture of elastomer base and curing agent (Sylgard 184, Dow Corning, United States) was prepared. It was stirred for 10-15 min to avoid streaks in the cured PDMS and degassed for 1.5 h to remove remaining bubbles. The PDMS mixture was poured onto the master, which was placed inside a large Petri dish. The mould was placed onto a hotplate for 3h at 95°C in order for the PDMS to cure completely. Finally, the hardened PDMS was cut along the reactor outlines and holes were punched with a surgical biopsy hole punch (EMS, Rapid core 1.2 mm) to create an inlet and outlet. To create a watertight seal, the PDMS is bonded to a glass microscope slide using a plasma cleaner (Harrick Plasma PDC-32G and PDC-VCG). This plasma treatment activates the surface and generates reactive chemical groups for covalent bonding[43], creating a permanent seal and rendering the PDMS temporarily hydrophilic. The sealed reactor is saturated with DI water using a pipette to avoid having air inside the reactor pore space, as this can cause bubbles during an experiment. After saturating the reactor with DI water to additionally keep the reactor from collapsing, tubing (Tygon, ND-100-80 Tubing - 0.5 mm

(0.02") ID x 1.52 mm (0.06") OD) was connected to both inlet and outlet. At this point, the reactor is assembled and can be used for further experiments or stored to be used later.

Integration of a reactive surface into the PDMS reactor

Table 3. Experimental conditions: showing the three different approaches tested to integrate a reactive surface into a "soil-on-a-chip"; including the reactor type, the minerals used and the method of mineral introduction

Reactor	Reactor Type	Mineral	Mineral introduction method
1. Mineral coated resin reactor	Resin reactor	Cr-minerals mixed with ethanol	Solution was sprayed onto reactor using a spray gun
2. Mineral embedded PDMS reactor	PDMS reactor	0.25% and 0.025% natural goethite powder	Directly mixed into the liquid PDMS, stirred and cured as described before
		0.025% Cr (III)oxide; 350 µl of 0.5 mM $CrOH_3$	
3. Pore space flooding PDMS reactor	PDMS reactor	aqueous suspension of goethite (1 mM)	Pore space flooding of reactor with mineral suspension (syringe pump)
		Cr(III)hydroxide suspension (0.1 M)	

Fabrication of mineral coated resin reactor

We tested three different approaches to create a reactive mineral surface inside the microfluidic reactor. The first approach to integrate a reactive surface into the pore space was a resin reactor model that was spray coated with minerals. This model was built by Arunima Bhattacharjee at the Pacific Northwest National Laboratory (PNNL). Using a Si wafer master with the desired pore space design, two reactors were fabricated using UV-curable polyurethane-based resin. After the reactors were fully cured and bonded to a regular microscope glass slide (75 mm x 25 mm x 1 mm), one was coated with Cr-minerals mixed with Ethanol using a spray gun. The other reactor was used as a blank to compare the extent of the mineral coating.

Fabrication of PDMS reactor embedded with mineral

As a second approach to develop mineral-embedded "soil-on-a-chip" models, we developed a reactor by mixing the PDMS base and the curing polymer at a 10:1 ratio and directly adding in minerals. Natural goethite powder was added at 0.25% and 0.025% and mixed well for 15 mins with a glass pipette. The mixture was degassed, poured into the microfluidic reactor master, and cured on the hotplate as described above. Additionally, two different methods were pursued using Cr mineral. Firstly, 0.025% of Chromium(III)oxide was directly added to the PDMS, and secondly, 350 µl of 0.5 mM $CrOH_3$

suspension (pH 7) was pipetted into the PDMS. All reactors were finalized as described in the section above.

Pore space flooding of PDMS reactor with mineral

The last approach to create a reactive surface inside the reactor pore space was to inject a controlled amount of mineral suspension into the reactor. For this method, a regular PDMS reactor was assembled as described in the section 'PDMS reactor fabrication protocol using soft lithography'. The reactor was connected to an inlet tube and an outlet tube. The inlet tubing was attached to a syringe and needle, introducing the mineral suspension into the pore space. The outlet tubing containing the effluent was collected in an Eppendorf tube (2 ml). The pore space flooding was conducted using a syringe pump to ensure an even and controlled distribution of the mineral suspensions at the rate of 1 ml per hour for 1 hour, for a total solution volume of 1 ml. This pore space flooding was conducted with an aqueous suspension of goethite (1 mM), prepared at a neutral pH and with a Chromium(III)hydroxide suspension (0.1 M), prepared at pH 7 (Appendix C). The dissolution of the minerals inside the reactor was tested by flushing DI water, reducing or oxidizing agents, and a ligand through the pore space. We used 0.1 M oxalic acid and 0.1 M Ethylenediaminetetraacetic acid (EDTA) adjusted to pH 7 with NaOH and stabilized with 10 mM HEPES buffer for the Fe oxide reactor and 100 µM manganese pyrophosphate (Mn-PP) for the Cr oxide reactor.

Optical microscopy imaging of all reactor types

All images were acquired with an inverted fluorescence microscope (Eclipse Ti2, Nikon) with a Lumencor LIDA light source and a Hamamatsu ORCA-Fusion camera. For all stitched images (1% overlap) of the entire microfluidic reactor, a 4x objective lens (1.62 microns/pixel) was used. For more detailed images of selected areas, we used a 10x objective (0.66 microns/pixel).

Image analysis

All acquired images were analysed using the MATLAB R2023a Software[44] for academic usage. The images were cropped (Matlab function *imcrop*), binarized (*imbinarize*) and the area of the minerals inside the pore space was calculated by creating a mask using the threshold function (*regionprops* and *bwareafilt*). The annotated Matlab code is provided in Appendix E.

Effluent analysis

The effluent samples collected in the pore space flooding approach were digested using an acid digestive solution (5% HNO_3, 25 mM oxalic acid). Equal amounts of sample (1 ml) and acid digestive solution (1 ml) were pipetted into 2 ml Eppendorf tubes and placed on a shaker for 18 h. After digesting, the samples were filtered using 0.22 µm PES syringe filters and diluted with 1% HNO_3 to a final volume of 10 ml. All samples were measured using an ICP-MS (Agilent 7900, Agilent Technologies, United States). The results were corrected according to the standards measured using the third order quadratic solver function in Excel[45].

Results and Discussion

Physico-chemical analysis and characterization of soil samples

The pH of the soil was determined to be 4.51, as shown in Table 3. Comparing the pH value measured to literature values, we observe that they are in a similar acidic range. Nanda et al. (2022) determined the pH of six different sites in the Sukinda Valley area between 4.07 and 5.49, supporting our findings. Additionally, the map (Figure 5) showing the soil pH of the Jajpur district as analysed by the International crops research institute for the semi-arid tropics (ICRISAT) reveals that most of the Sukinda area soil pH ranges between "strong to very strong acidic" with a small exception showing a moderate pH[47]. The acidic pH is explained by the close vicinity to the mining activities. Soils close to mining activities are always associated with metals and runoffs. As a result, mine soils like overburden and quarry tend to be low in pH and deficient in all nutrients. Plant macro- and micronutrients might be leached out due to the acidic pH of the ground. This influences plant growth and dictates crop yields in the affected area[46]. Another factor that was measured was the oxygen content of the paddy soil. It was 0.23 mg/l, which corresponds to 2.4% of oxygen in the sample. This value indicated a very low oxygen content in the soil sample. A soil oxygen measurement gives important information about the soil climate as oxygen plays an important role in plant growth and SOC mineralisation[48]. Here, paddy fields are a unique system that has experienced periodic changes in oxygen availability due to intentional flooding practices.

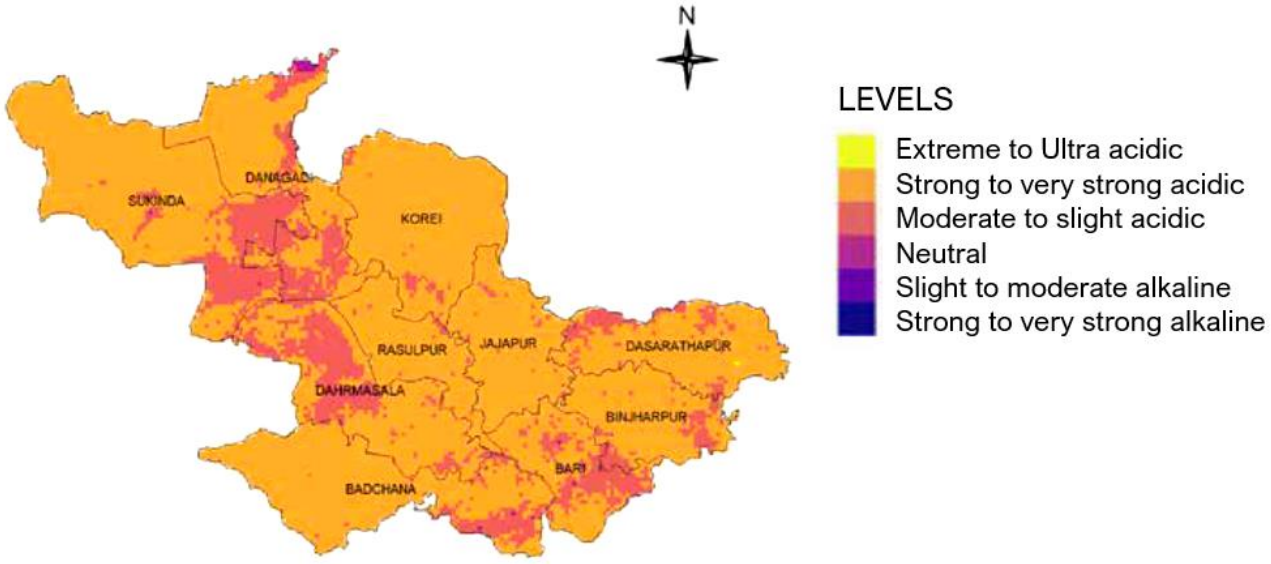

Figure 5. The pH range of soils in the Jajpur district, including the Sukinda area conducted by the International crops research institute for the semi-arid tropics (ICRISAT). Image obtained from ICRISAT report 2020.

The total organic carbon (TOC) and nitrogen content of the soil were 1.70% and 0.25%, respectively (Table 3). Here, the literature would suggest lower values regarding the carbon content specific to the area. Babu et al. (2017) found that the mean surface soil carbon content (SOC) ranged between 0.13% to 0.78%. Similar findings were reported in the paper from Das et al. (2013), stating that organic carbon

and nitrogen levels of the Odisha soil samples were extremely low. Matching results are depicted in Figure 6, showing the organic carbon content (%) as analysed by ICRISAT for the Jajpur district[47]. The higher value of 1.70% can be explained by the fact that the soil is used as an agricultural site, which means that local farmers are managing the SOC by adding off-farm organic residues such as manures, char and straw. This practice can increase the total organic carbon available in soil[50]. Another explanation for the higher TOC value is the basic properties of paddy soil. They differ from arable upland soil because paddy soil is intentionally flooded and tilled under water saturated conditions. These anaerobic conditions allow a very slow decomposition of organic matter, which in turn is beneficial to the soil organic matter accumulation[51]. The total nitrogen content with a value of 0.25% is also on the lower end of the normal range. Sadej and Przekwas (2008) suggested that nitrogen forms that are available to plants in soil are generally low, between 1-5%. A study conducted close to the Sukinda chromite mine reported total nitrogen levels between 0.01% and 0.03%, additionally supporting the extremely low value ranges in the region of interest[9].

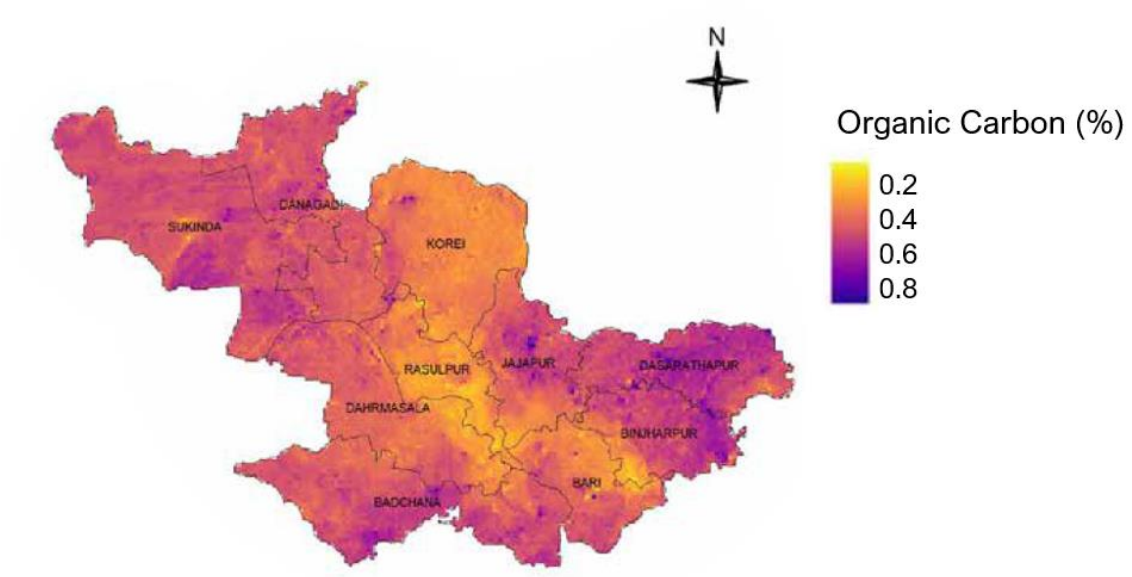

Figure 6. The organic carbon content in soil of the Jajpur district, including the Sukinda area conducted by the International crops research institute for the semi-arid tropics (ICRISAT). Image obtained from ICRISAT report 2020.

Table 4. Physiochemical properties of the paddy soil before fertilization and planting (n=3).

Parameters	Paddy soil
pH	4.51
Oxygen content	0.23 mg/l (2.4%)
TOC	1.70%
TN	0.25%

Note: TOC, Total organic carbon; TN, Total nitrogen;

Mineralogical study of the soil samples

A mineralogical characterization of the soil samples from the Sukinda Valley, close to the chromite mine, was carried out using extraction and digestion protocols, as well as an X-ray diffraction scan.

XRD analysis

The soil collected from the study site in the Sukinda Valley had a muddy, clayey, rocky nature. The colours of the soil were mainly brick, red, and brown. For the sieved, homogenized soil samples, XRD studies were carried out. These samples contain mainly silicates (SiO_2), as shown in Figure 7, but small amounts of kaolinite, illite, and Muscovite were also detected. Comparing the findings with previous soil studies from this region shows that a high amount of quartz is very typical. Das et al. (2013) performed several XRD studies using soil collected in the Sukinda region. Their samples revealed a composition of chromite, hematite, goethite and quartz, with some samples also containing Kaolinite. Additionally, Aluminium phosphate ($AlPO_4$) was detected, as depicted in Figure 8, which might be a product of transformed phosphorous fertilizer in acidic soil[53].

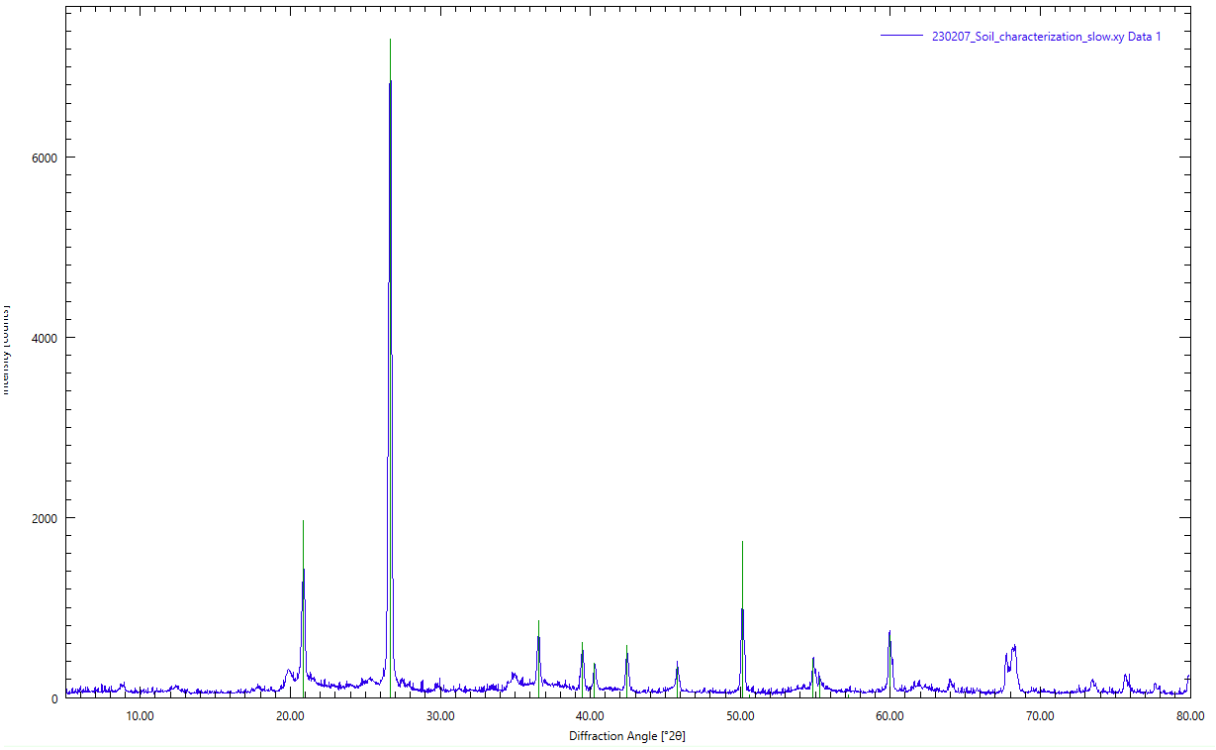

Figure 7. X-ray diffraction pattern of Sukinda Valley soil samples depicting the presence of quartz (SiO_2)

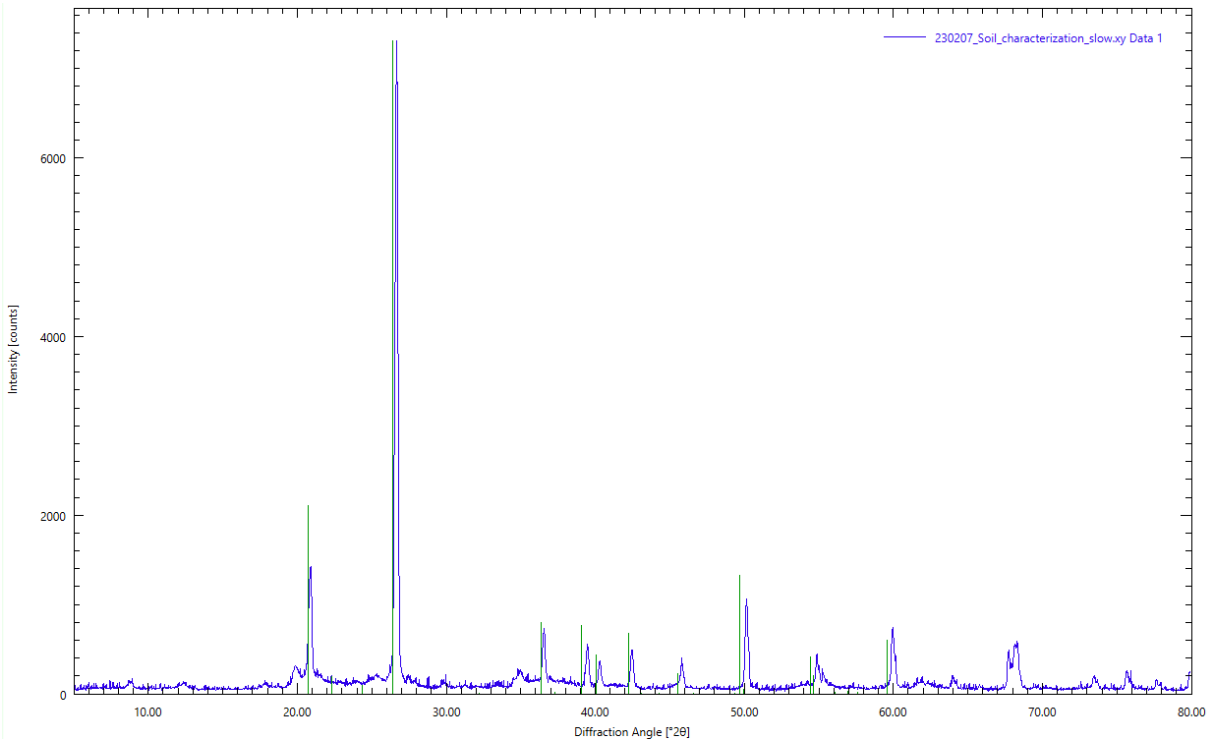

Figure 8. X-ray diffraction pattern of Sukinda Valley soil samples depicting the presence of Aluminium phosphate ($AlPO_4$)

Sequential extraction according to Hasan et al. (2018)

The possible environmental mobility and bioavailability of heavy metals in soil are determined by chemical speciation. A full understanding of the physicochemical forms of heavy metals is necessary to comprehend their environmental behavior, including their mobility, bioavailability, and paths in soil. Fractionation and sequential extraction techniques are frequently used on soils to determine their chemical phase association. Variations in the oxidation state, soil pH, temperature, redox potential, decomposition of soil organic matter, and other factors significantly impact the substance's essentiality, toxicity, and bioavailability[54]. The sequential extraction consists of a series of chemical extraction steps, each being different in nature and more severe compared to the previous one. The analysed phases (adapted from Hasan et al. (2018)) include the exchangeable (weak acid soluble) fraction, the reducible (Fe and Mn oxide bound) fraction, the oxidisable (organic matter bound) fraction and the residual (non-silica bound) fraction. In general, the metals found in the exchangeable, oxidizable, and reducible fraction are readily available or become available when the acidity or salinity in soil increases. The residual fraction, however, is assumed to be unavailable under normal environmental conditions[55]. To obtain an overview of the amount of Cr, Fe and Mn bound to different phases in soil the sequential extraction according to Hasan et. al, 2018 was carried out. As shown in a cluster analysis by a similar study, Cr, Fe, and Mn, also obtained from Sukinda Valley soil, are closely related to each other, making it essential to analyse all three elements[9]. The amount of each element related to the fractionation is shown in Table 4.

Regarding the different extraction steps, the concentration of Cr in the exchangeable / carbonate-bound fraction is relatively small. This shows that most of the Cr present in the soil samples is not weakly absorbed and retained on the soil surface. With the analysis of the second phase, it becomes clear that only a very small amount of Cr is bound to Mn and Fe-oxides in the soil. The highest amount of Cr extracted was in the residual phase (144.21 mg/kg), making up to 89.2% of the total Cr extracted, followed by the oxidizable fraction (13.75 mg/kg), which is 8.5% of the total Cr value. A similar trend was observed by Hasan et al. (2018). The amount of Cr in the oxidizable fraction translates to 8.5% of Cr in the soil sample, which is bound to various forms of organic matter. Because organic matter in the soil functions as an electron donor, it creates the ideal environment for Cr(VI) to be reduced to Cr(III). Additionally, the breakdown process of organic substances ingested by microorganisms can result in the release of organic acids and a drop in pH. This would impact Cr speciation because Cr(III) is more prevalent at a lower pH. The Cr(III) formed has the ability to form soluble organic complexes that are mobile in nature and can be related to the relatively high levels of organic bound Cr in this fraction[54]. Results of the amount of Cr in the residual fraction suggest that most of the Cr in the soil sample is part of a chemically inert fraction that is inaccessible to biota because it is fully immobile in nature. Vollprecht et al. (2020) analysed the mineralogical bonding of metals in soil and found that with around 87% of Cr bound to the residual fraction, consequently, Cr is the least mobile metal. Metals from anthropogenic inputs are typically found in the first four fractions, whereas the parent rock naturally contains the metals found in the residual fraction. Consequently, Cr speciation is critical for research on Cr mobility[54].

The distribution of iron in the soil sample was in the following decreasing order: residual > exchangeable > oxidisable > reducible. The high value of Fe in the residual phase points to a stable association of Fe as a mineral matrix in the soil, which is indicative of a mineral origin of Fe[57]. This fraction is not bioavailable. The percentage of Fe present in the other three fractions is very similar, ranging between 11.3% and 15.9%. Results show that 15.9% are weakly adsorbed and retained on the soil surface by weak electrostatic interactions, 11.3% are associated with Fe and Mn oxides, and 13.4% are bound to organic matter.

Manganese (Mn) exhibited the following decreasing order for the metal concentration in each fraction: residual > reducible > exchangeable > oxidisable. Consistent with the relatively high fraction of Mn in the residual phase, the largest part of Mn from the Mn ore deposits in the Odisha district mainly occurs as metamorphosed bedded sedimentary deposits [57]. Regarding the remaining three fractions, 22.1% are in the exchangeable fraction and can be easily released by ion-exchange processes or co-precipitate with carbonates; 30.8% are released under reducing conditions, and 4.7% are removed from soil under oxidizing conditions. As the sequential extraction protocol chosen in this study was specified to analyse Cr in the different phases, the results for the other metals might be more accurate when using a specific sequential extraction protocol, e.g., for iron and manganese.

Table 5. Statistical distribution parameters for selected metal concentrations (mg/kg) in soil.

		Cr		*Fe*		*Mn*	
Exchangeable	Mean	2.15	1.4%	5500	15.9%	173.3	22.1%
	SD	0.97		3711		44.9	
Reducible	Mean	1.48	0.9%	3921	11.3%	241.2	30.8%
	SD	1.2		560		22.4	
Oxidisable	Mean	13.75	8.5%	4629	13.4%	36.5	4.7%
	SD	2.7		2546		4.7	
Residual	Mean	144.21	89.2%	20530	59.4%	331.9	42.4%
	SD	13.7		2195		21.9	
Pseudo-total		161.59	100%	34582	100%	782.9	100%

Aqua regia digest

Additionally, an Aqua Regia digestion was conducted to analyse multiple elements present in the soil (Table 5). Overall, the mean metal concentrations exhibited the following increasing order: Cu < As < Ni < S < Cr < P < Mn < Mg < Ca < Zn < Al < Fe. With values ranging from 8.8 mg/kg for Copper and 38385 mg/kg for iron. The high iron, aluminium, calcium and magnesium values in the soil samples relate to the presence of the minerals chromite, goethite and hematite. The lithography of the Sukinda Chromite Belt is shown in Figure 9.

Table 6. Statistical distribution parameters for selected metal concentrations (mg/kg) in soil.

	Al	*As*	*Ca*	*Cu*	*Cr*	*Fe*	*Mg*	*Mn*	*Ni*	*P*	*S*	*Zn*
Min	24323	6.2	1077	7.8	206	36674	1516	284	12.5	204	149	8083
Max	24347	16.5	2246	10.6	212	40407	1551	299	23.9	248	234	9252
Mean	**24335**	**11.3**	**1829**	**8.8**	**209**	**38385**	**1532**	**291**	**18.5**	**227**	**180**	**8663**
Confidence level (95%)	35.2	14.5	1304	3.1	6.1	3771	34.6	15.2	11.5	44.1	93.7	116.9
Coefficient of variation	0.001	1.27	0.71	0.35	0.029	0.098	0.023	0.052	0.61	0.194	0.519	0.135

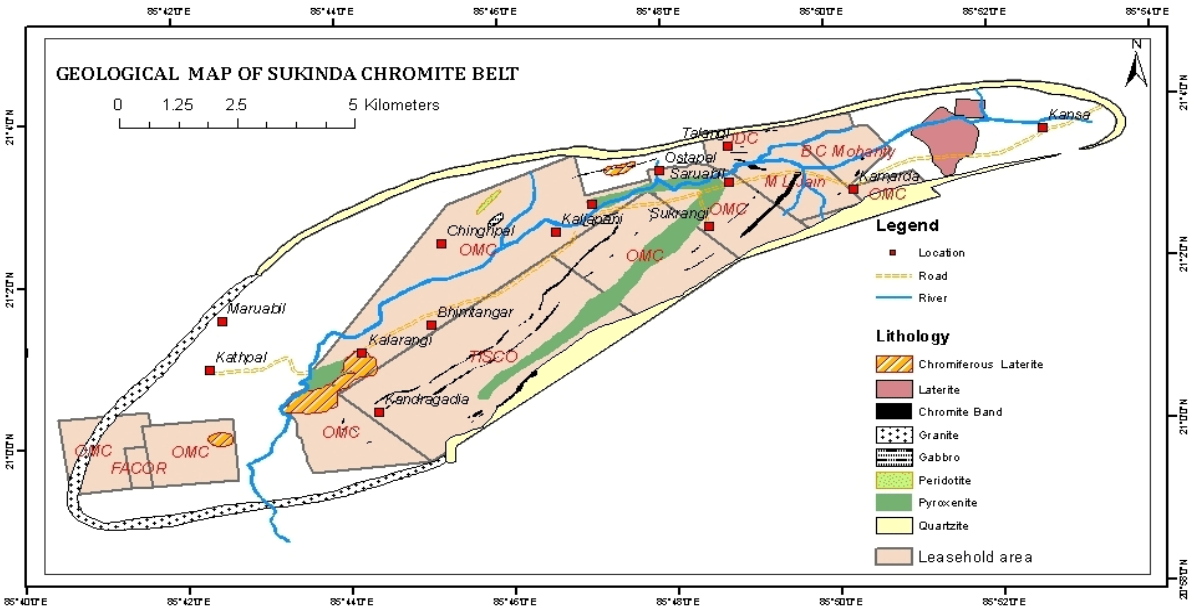

Figure 9. Geological map of the Sukinda Chromite belt (Image obtained from Directorate of Geology, Government of Odisha)

With this soil analysis, a general overview of the soil properties was established. Additionally, the contamination levels and composition of the soil sample were investigated; the origin, mobility, and speciation of Cr in soil were also revealed. These provide fundamental information for further batch and rice planting experiments.

Batch dissolution experiment

Chromium-ligand complexes have been recognized by the scientific community for almost 50 years, but only a few studies have tested the interaction between them and the impacts they have on the environmental chemistry. A series of batch dissolution experiments were conducted to gain a better understanding of the possible effects that ligands have on chromium mobility and availability. Furthermore, to choose the appropriate ligands and concentrations for the following pot experiment, two different batch dissolution experiments were carried out.

Chromium dissolution rates for the model compound $Cr(OH)_3$

Firstly, the Cr dissolution rate for the model compound Cr hydroxide was analysed using 1 mM citric acid and 0.1 mM DFOB, with an initial solution pH of 7 (buffered with HEPES). The experimental conditions were chosen so that the amount of total Cr hydroxide exceeded the added chelating agent in order to only dissolve a small amount of $Cr(OH)_3$. As shown in Figure 10, a higher dissolution of Cr hydroxide can be observed with citric acid present in the system compared to the control group. After 456 h, the mean total Cr concentration reached 81.4 ppb (1.57 µM). These findings are consistent with previous studies, showing that the chelating agent citric acid effectively dissolves amorphous chromium hydroxide[28, 58]. Additionally, other findings support the observed dissolution rate, stating that only a small amount of $Cr(OH)_3$ dissolution happens in the first 96 h, and the majority of the reaction takes place after that[28]. This can be explained by the general mechanism of the process. After adding the

polydentate ligand citric acid to the $Cr(OH)_3$, the chelation process, where the ligand bonds to the metal ion and forms a ring, takes place[24]. Here, only very small amounts of free ligand and dissolved Cr can be measured, as the metal ion in solution does not exist on its own but in combination with the ligand, forming a chelate complex[59]. This process is described in Equation 1, where the central metal ion (Me) forms a complex with the ligand (L) on the base of Lewis acid-base interaction[60 61].

Equation 1

$$Me + L \leftrightarrow MeL$$

As shown in Figure 10, after the initial complex formation, the measured Cr in solution increases. This is due to the fact that complex formation can significantly raise the solubility of salts that are only weakly soluble. The solubility increases, the larger the complex formation constant (K_f) (Equation 2) is, the higher the ligand concentration is[60 61].

Equation 2

$$K(f) = \frac{[MeL]}{[Me][L]}$$

Another important factor for the ligand induced dissolution of Cr hydroxide is the pH. In many sparingly soluble salts, the anion is the conjugate base of a weak acid. Protonation of the anion at low pH can significantly increase the salt's solubility. Oxides can be classified as acidic oxides, basic oxides or amphoteric oxides. Chromium(III)-hydroxide is an example of an amphoteric oxide; it is soluble in both basic and acidic solutions[62].

Figure 11 shows the Cr dissolution rate after adding the siderophore desferrioxamine B. The concentration of total Cr was higher with DFOB compared to the control experiment, but the total dissolution rate is quite low. This can be explained by the fact that for siderophores, the dissolution rates increase by 10-fold when the concentration of the siderophore is increased by the same factor. This suggests a proportional relationship between siderophore concentration and dissolution rate[26]. Duckworth et al. (2014) proved that with a higher concentration of DFOB (25 mM), a total dissolved Cr concentration of ~780 ppb (15 µM) can be measured after 250 hours.

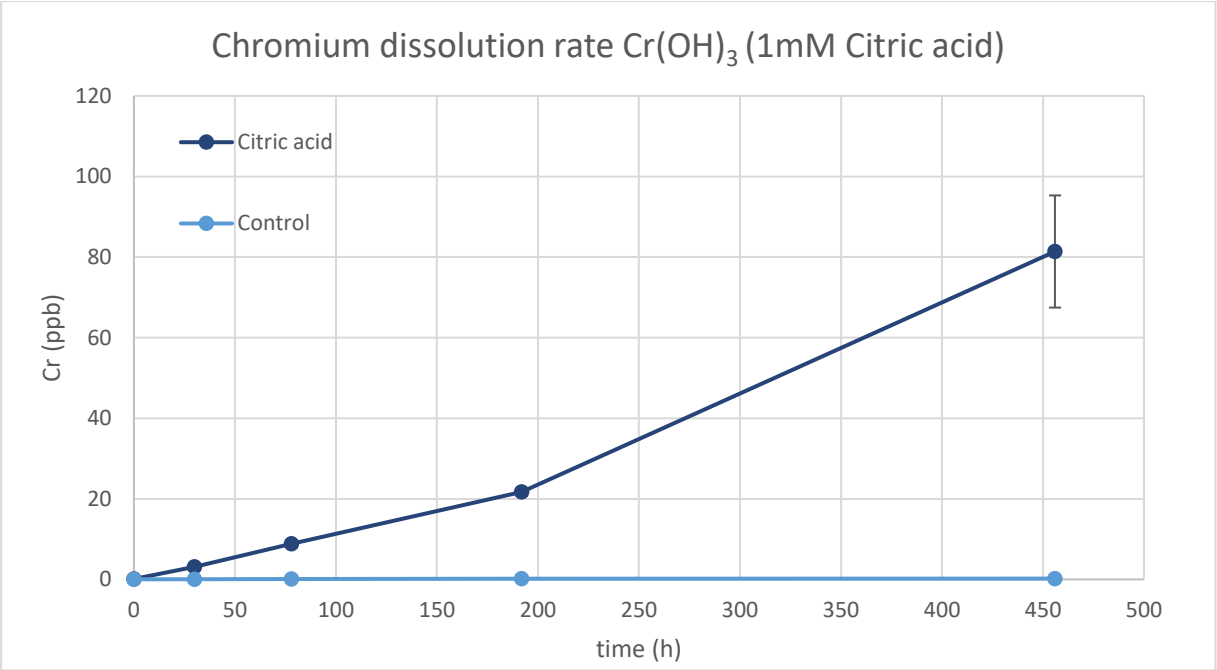

Figure 10. Chromium dissolution rate $Cr(OH)_3$ – 1 mM citric acid

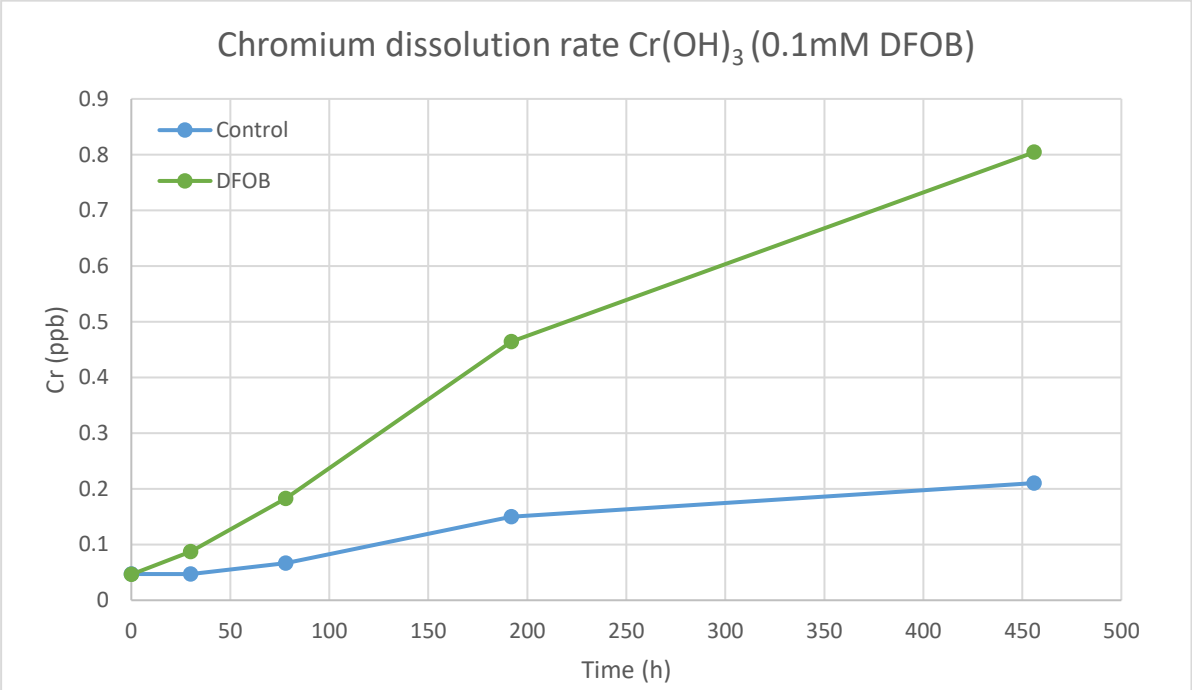

Figure 11. Chromium dissolution rate $Cr(OH)_3$ – 0.1 mM DFOB

Chromium dissolution rates for the Cr-containing soil samples

As a follow-up experiment, the Cr-contaminated soil samples were used to determine if ligand induced Cr-dissolution takes place in a more complex system where other elements such as Fe and Mn are present. Three different types of ligands at three different concentration levels were tested.

Firstly, 0.1 mM DFOB was added to a 1 g-100 ml soil to solution ratio with 30 mM NaCl as electrolyte at a pH of 7. The results are shown in Figure 12. In the absence of DFOB, the dissolved Cr remained

under a value of 5 ppb (0.1 µM) over the course of the experiment. With the addition of the siderophore, the dissolved Cr reached 71 ppb (1.4 µM) after 456 hours. This outcome shows that in the presence of desferrioxamine B, Cr is released from the solid phase. These results are in agreement with Saad et al. (2017). In their case, 0.1 mM DFOB resulted in 1.5 µM dissolved Cr in 360 hours, with a Cr release rate of 4.8 x 10^{-14} mol m^{-2} s^{-1}. Compared to other siderophores, like enterobactin or pyoverdine, DFOB resulted in the smallest amount of released Cr with the slowest dissolution rate[30].

Secondly, 1 mM citric acid was added to a 1 g-100 ml soil to solution ratio containing 30 mM NaCl as electrolyte at a pH of 7. The results are shown in Figure 13. Also, for this batch, in the absence of citric acid, dissolved Cr concentration remained under 5 ppb (0.1 µM) throughout the experiment. After adding the organic acid, we see an increase in dissolved Cr, reaching the highest concentration after 456 hours with a value of 59 ppb (1.1 µM). Here, the literature suggested an even higher extent of ligand promoted dissolution of Cr. In previous studies, the addition of 0.1 mM citric acid yielded in 3.5 µM dissolved Cr over the time course of 360 hours during the experiments [30]. This study determined the Cr dissolution rate for citric acid at 1.6 x 10^{-13} mol m^{-2} s^{-1}.

Lastly, 10 mM oxalic acid was added to 1 g-100 ml soil to solution ratio containing 30 mM NaCl as electrolyte at a pH of 7. The same experimental parameters were used to study the effect of pH, so a second batch was conducted at pH ~2. The results are depicted in Figure 14. In the absence of the ligand oxalic acid, dissolved Cr remained under a value of 5 ppb (0.1 µM) throughout the experiment. The first result that becomes clear is that in both cases (pH 2 and pH 7), a Cr release from soil can be observed. The higher ligand concentration resulted in higher total Cr values at pH 2. Furthermore, a difference can be seen between the two pH scenarios. The lower pH simulation resulted in an 8× higher Cr dissolution compared to the neutral pH of 7. Here, the greatest value of 166 ppb (3.2 µM) was reached after 456 hours. For the neutral pH, a value of 26 ppb (0.5 µM) was recorded after the same time period. The literature agrees with the general trend of the ligand promoted Cr dissolution by oxalic acid, whilst Saad et al. (2014) again observed higher levels of total dissolved Cr at a lower oxalic acid concentration, with a Cr dissolution rate of 6.5 x 10^{-14} mol m^{-2} s^{-1}. Their findings support our observations that citric acid caused the greatest dissolution of Cr, followed by oxalic acid and, lastly, DFOB.

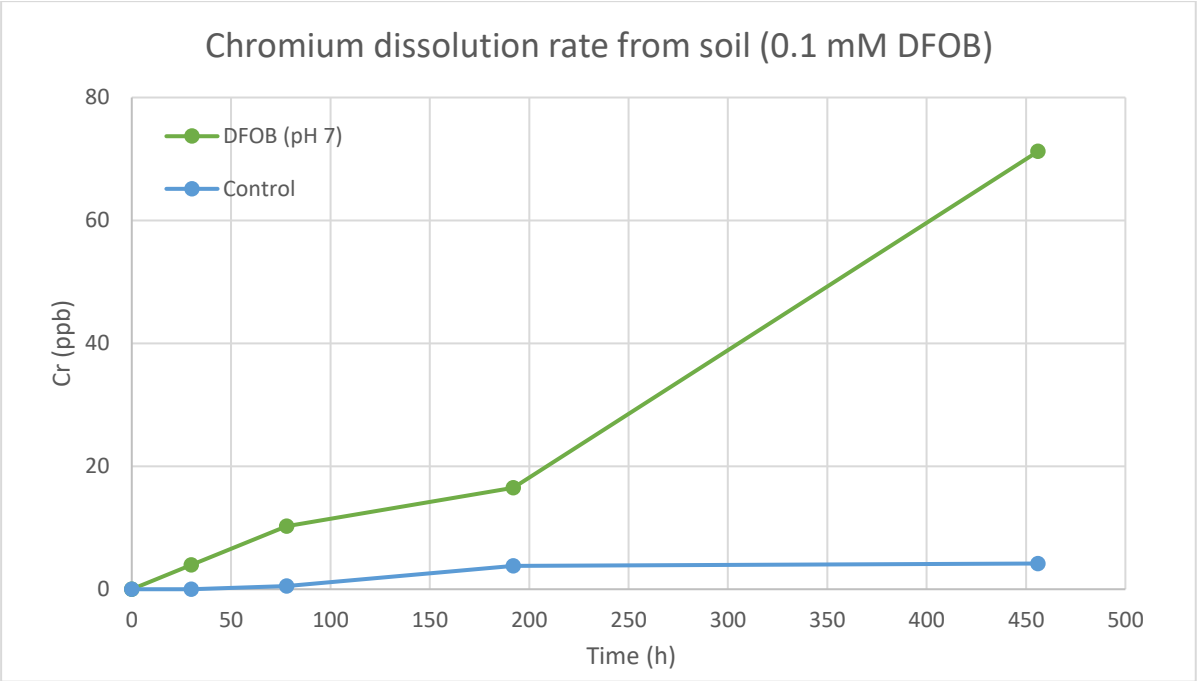

Figure 12. Chromium dissolution rate from soil - 0.1 mM DFOB

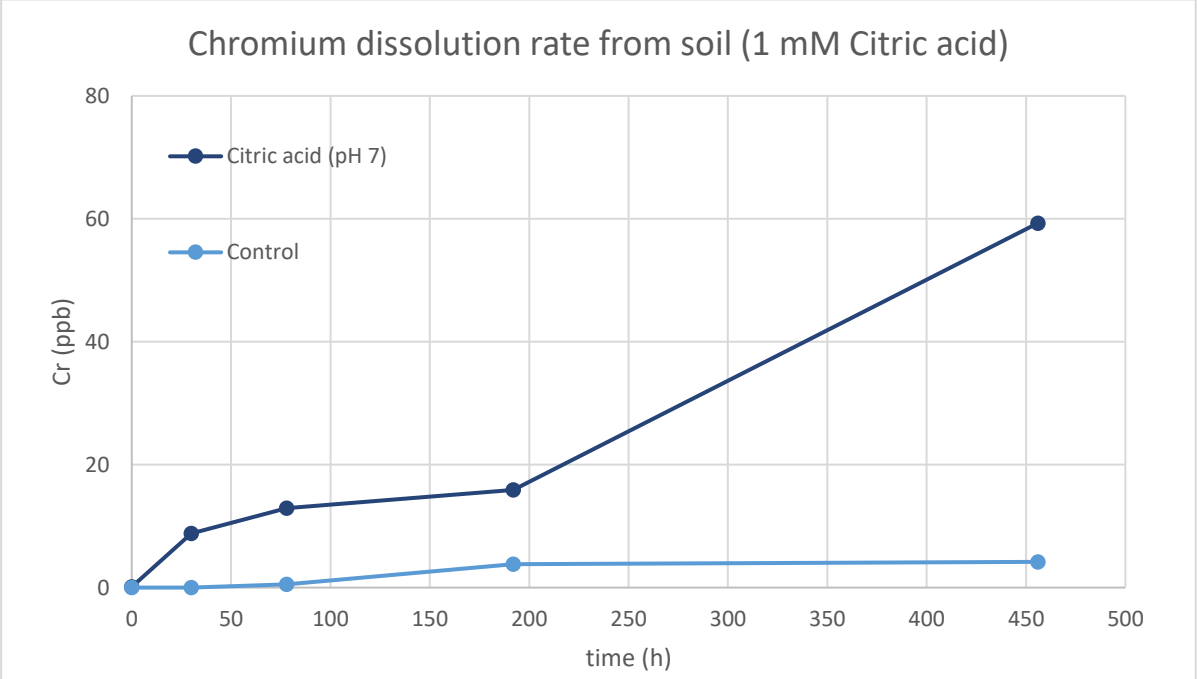

Figure 13. Chromium dissolution rate from soil – 1 mM citric acid

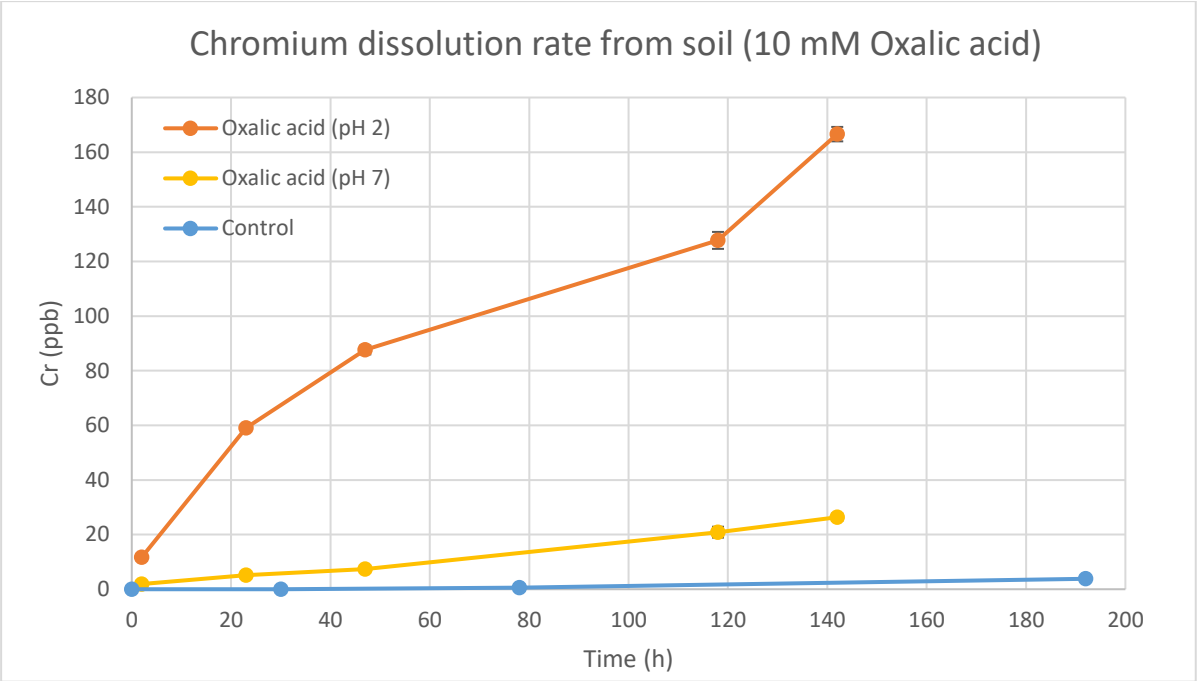

Figure 14. Chromium dissolution rates from soil – 10 mM oxalic acid

These two batch experiments, conducted using the model compound $Cr(OH)_3$ and the Cr-contaminated soil sampled, combined with the literature, suggest that both the organic acids citric acid and oxalic acid, as well as the siderophore DFOB have the ability to induce Cr dissolution even if in reducing conditions where Cr is thought to be immobilised. Based on these experiments as well as literature results, certain types and concentrations of organic ligands were chosen to conduct the rice planting experiment.

Rice planting pot experiment

DFOB addition: Ligand induced Cr dissolution in a Paddy system

Results of the analyses of the first ligand treatment (DFOB addition) to the paddy system show that only a very small amount of Cr was dissolved from the soil over the course of the experiment. Aqueous Cr concentrations for all three replicates remained under 1.2 ppb for all five sampling points, as shown in Figure 15.

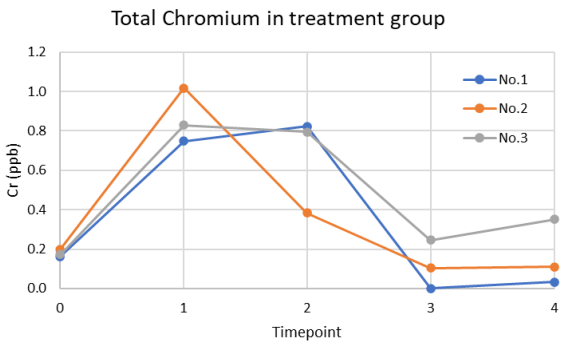

Figure 15. Measured total Chromium with DFOB addition for the treatment group over five distinct sampling points

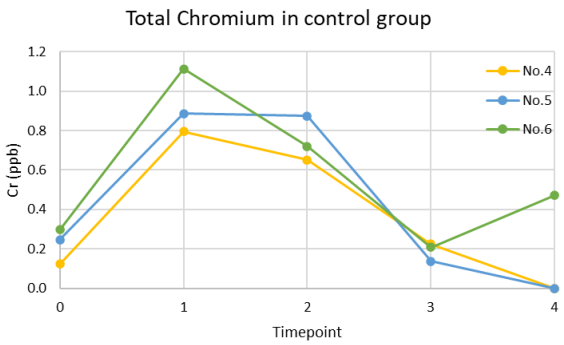

Figure 16. Measured total Chromium of the control group over five distinct sampling points

Comparing the ligand-treatment group (Figure 16) to the control group, no significant difference could be observed for the total dissolved Cr measured with the Rhizon porewater samplers in this system. Considering the Cr concentrations measured in the bulk soil, it is possible to calculate the percentage of Cr released from the solid phase. Note that only the exchangeable fraction is bioavailable, and the reducible and oxidizable fractions are potentially mobile; we compare the measured dissolved Cr in this experiment to results from the sequential extraction (SE) excluding the residual phase. The first three phases from the SE yielded 17.4 ppm of Cr in the soil, whereas the treatment group reached a total Cr value of approx. 2ppb over the entire period of the experiment, as shown in Table 6. This shows that only 0.01% of the bioavailable and potentially mobile Cr in the soil system was released during the DFOB treatment. No relationship between the addition of DFOB and the measured potentially mobilized Cr could be determined in this study. One potential reason for this outcome is the slightly higher affinity DFOB has for iron than chromium, meaning that once the ligand enters the system, it is more likely to form a complex with Fe, causing a competition effect. Literature speculates that Cr(III) may have a comparably high stability constant with DFOB, $K_{Cr(III)\text{-}DFOB} = \sim 10^{30.6}$. The reported stability constant for Fe(III)-DFOB complex is $K_{Fe(III)\text{-}DFOB} = 10^{32.063}$ [64]. Note, however, that due partly to analytical difficulties, there have been no experimental approaches determining the stability constant between Cr(III) and DFOB. A study by Saad et al. (2017) reported that in the presence of DFOB, Fe was released at higher rates and to a greater extent than Cr from all solid phases.

Table 7. Total measured Chromium [ppb] for each sampling point (0-4) for the treatment group (No.1-3) and Control group (No.4-6), the calculated total concentration from each sample over the course of the experiment and the average for the treatment group and the control group after DFOB addition.

	Treatment group			Control group		
Timepoint	No.1	No2.	No.3	No.4	No.5	No.6
0	0.16	0.20	0.17	0.12	0.25	0.30
1	0.75	1.02	0.83	0.79	0.89	1.11
2	0.82	0.38	0.79	0.65	0.87	0.72
3	0.00	0.10	0.25	0.22	0.14	0.21
4	0.03	0.11	0.35	0.00	0.00	0.47
Total Cr	1.77	1.81	2.39	1.79	2.14	2.81
Average of Total Cr			1.99			2.25

These results indicate that multiple factors can play an important role in the paddy soil system; DFOB has the ability to dissolve Cr from soil, but this was not clearly evidenced in pot experiments.

DFOB addition: Effect of pH, Eh and OM on Chromium bioavailability and speciation

Another factor that influences Cr mobility from the soil is the pH of the system. Here, the results, as shown in Figure 17, indicate that after the DFOB addition to the system, the pH increased from 5.5 to 6.5 and then went back to the original value. With the control group (Figure 18), we also see fluctuations in the pH over time but not a specific cluster as we observe for the treatment group. Multiple reasons can explain the changes in pH. Generally, the pH of the soil is determined by the minerals present in the parent material of the soil. As discussed in the section above, the pH of the Sukinda region is usually around 5-6 and fluctuates during the seasons[47]. This is due to the very humid environment, warm temperatures, and the monsoon. These events drive the process of soil acidification due to the leaching and weathering of soil minerals[65]. All these conditions were replicated in the experiment using a climate chamber, where the humidity was set to 75% and the temperature between 26-28°C. As the pH for both groups stays below 7 throughout the experiment, the type of environment is acidic[66]. In acidic solutions, Cr(III) may be the dominant species, as Cr(VI) can be easily reduced under these conditions. Additionally, decreasing the pH in the soil system can promote the release and mobilisation of Cr(III)[21]. For this experiment, however, no correlation between the pH and the measured dissolved Cr concentrations could be detected.

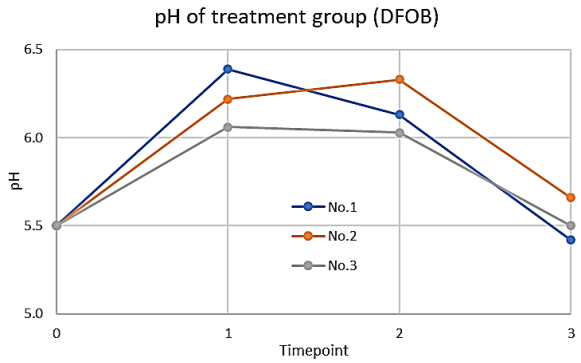

Figure 17. Measured pH of the treatment group with DFOB addition over four distinct sampling points

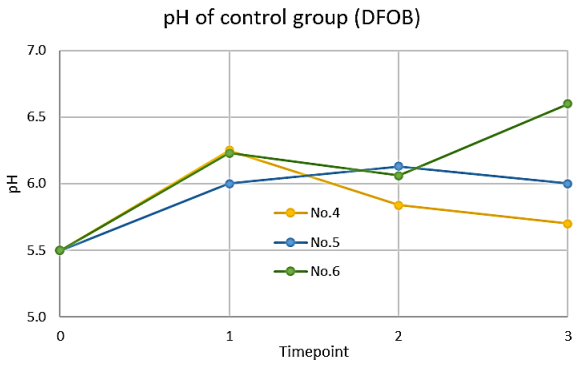

Figure 18. Measured pH of the control group with DFOB addition over four distinct sampling points

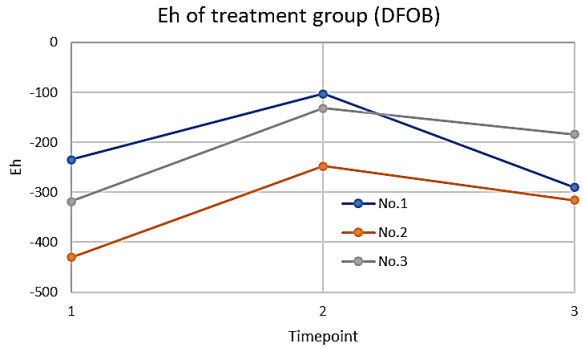

Figure 19. Measured Eh of the treatment group with DFOB addition over three distinct sampling points

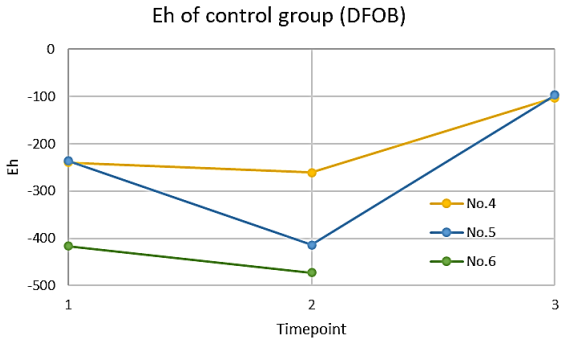

Figure 20. Measured Eh of the control group with DFOB addition over three distinct sampling points

Another factor that should be monitored during the experiment is the Eh value of the soil system, as Cr species are very sensitive to the redox fluctuations[67]. The redox potential of the soil is categorized into three types of environments. Firstly, the aerobic environment has an Eh value over 350 mV, where Cr(VI) would be the dominant speciation. Secondly, the suboxic environment (350 mV > Eh > 100 mV), where the Cr speciation is highly pH dependent. And lastly, the anaerobic environment (Eh < 100 mV) where the toxic Cr (VI) is readily reduced to the non-toxic Cr(III). However, whether Cr(VI) can be completely reduced to Cr(III) and whether Cr(VI) can be re-generated in anaerobic environments remain controversial. According to Xiao et al. (2015), even under continuous flooding conditions, a significant amount of Cr(VI) remained in paddy soils with only a slight decrease. Changes in the soil redox state frequently occur during intermittent flooding and drainage in a series of sequential redox reactions, including Mn(IV), Fe(III), sulphate reduction, and methanogenesis. These factors may influence the conversion of Cr(VI) to Cr(III) under soil flooding conditions, either directly or indirectly[68]. Despite significant efforts to elucidate the oxidation-reduction cycles of Cr(III) and Cr(VI) in soils, explanations for the transformations between Cr(III) and Cr(VI) remain unresolved. In our case the main Cr speciation would be Cr^{3+}, $Cr(OH)_2^+$, $Cr(OH)^{2+}$, $Cr(OH)_3$ and $[Cr(OH)_4^-]$[21]. As shown in Figures 19 and 20, the

redox potential of the paddy system in the experiment was negative for both the treatment group and the control group. This is a result of the continuous flooding that was simulated during the rice growing. In this particular case, the Cr species present in soil can form insoluble chelates with oxygen, hydroxide and sulphate, be absorbed by Mn and Fe oxides, or form precipitates with organic matter and soil colloids. These chelates and precipitates would have a low bioavailability, which means that they are not easily taken up by the rice plants[21]. These processes would explain the very low dissolved Cr concentrations as observed in soil porewater within this system. Another factor that might additionally retain Cr(III) species in the soil is the organic matter (OM) content. Through different pathways, OM can control the speciation and bioavailability of Cr. Firstly, as soil organic matter has a high cation exchange capacity, it can form organic molecules and humic substances with Cr ions. Secondly, dissolved organic carbon can promote the reduction of Cr(VI) to Cr(III) via electron donation. Lastly, by exhilarating microbial activity and growth, it indirectly changes the conditions of the soil to a reducing environment by driving the biological reduction of Cr(VI)[21].

Oxalic acid addition: Ligand induced Cr dissolution in a Paddy system

As discussed in the paragraph above, many different scenarios could have influenced the speciation, mobilization or retainment and the bioavailability of Cr in soil. In order to compare the results that were obtained with the addition of DFOB to the paddy system, a second experiment was conducted. After a seven-day break to wash out the remaining ligand in the pots, a new ligand, oxalic acid, was added. As the results from the previous test showed no significant Cr mobilization with the amount of ligand (DFOB) that was added, a higher concentration of 10 mM was chosen for oxalic acid. Additionally, two different porewater samples were taken at each time point, one sample very close to the roots of the rice plant (Figure 21) and one taken from the bulk soil further away from the roots (Figure 23). Again, the control group did not receive any ligand over the course of the experiment and was monitored in the same way as the ligand-treatment group, as shown in Figures 22 and 24. By analysing the aqueous Cr that was sampled from both close to the rhizosphere and the porewater of the bulk soil, an increase in dissolved Cr concentration was observed. Over the course of the experiment, a porewater Cr concentration of 20.4 ppb was measured from within the rhizosphere and 21.6 ppb from the bulk soil (Table 7). By comparing these results with the previously determined dissolved Cr with DFOB addition (as discussed above), there appears to be an increase in dissolved Cr concentration by one order of magnitude. If the relationship of the ligand concentration and the dissolution is proportional by the same factor, the extent of Cr dissolution would be expected to be 100 times greater as we increased the ligand concentration by a factor of 100. Here, only an increase by 10 × was detected after the addition of oxalic acid, which is equivalent to approximately 0.1% of the total Cr in the bulk soil that was released. This can be explained by other influencing factors like pH, Eh, OM content and the presence of other minerals, retaining Cr in the solid phase. Nevertheless, comparing the Cr values of the treatment group to the control group, ligand induced Cr dissolution can be clearly observed despite the complexity of the system; the mean Cr concentration of the control group stayed below 1 ppb during the study. No clear

similarity or difference between the porewater measurement from within the rhizosphere and from the bulk soil can be detected. This might be due to the fact that the root mesh was completely distributed throughout the experimental pot, making it nearly impossible to categorize an area without roots.

Table 8. Total measured Chromium [ppb] for each sampling point (4-7) for the treatment group (No.1-3) and Control group (No.4-6) divided into rhizosphere sample and bulk soil sample, the calculated total concentration from each sample over the course of the experiment and the average for the treatment group and the control group after oxalic acid addition.

	Treatment group						Control group					
Timepoint	No.1		No2.		No.3		No.4		No.5		No.6	
	Rhizo	Bulk	Rhizo	Bulk	Rhizo	Bulk	Rhizo	Bulk	Rhizo	Bulk	Rhizo	Bulk
4	0.03	0.00	0.11	0.28	0.35	0.21	0.00	0.00	0.00	0.00	0.47	0.03
5	6.58	8.63	4.06	2.40	4.49	3.67	0.32	0.74	0.01	0.03	1.16	1.28
6	19.4	15.7	10.7	8.03	13.5	17.1	0.00	0.23	0.00	0.00	0.00	0.12
7	1.30	2.23	0.83	0.50	0.00	6.04	0.33	0.00	0.00	0.08	0.00	0.00
Total Cr	27.3	26.5	15.7	11.2	18.3	27.1	0.65	0.97	0.01	0.11	1.63	1.43
Average of Total Cr	20.4	21.6					0.76	0.84				

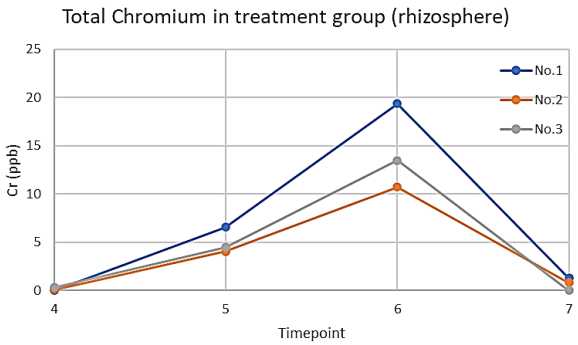

Figure 21. Total measured Chromium of the treatment group with oxalic acid addition over four distinct sampling points (rhizosphere)

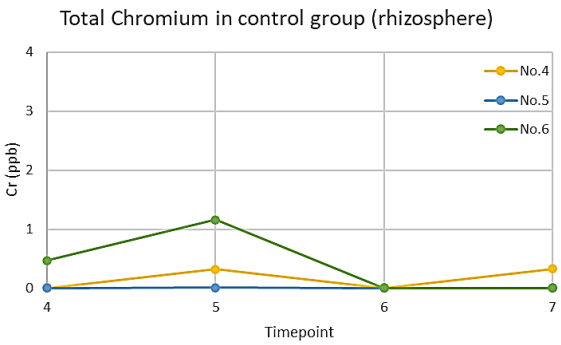

Figure 22. Total measured Chromium of the control group over four distinct sampling points (rhizosphere)

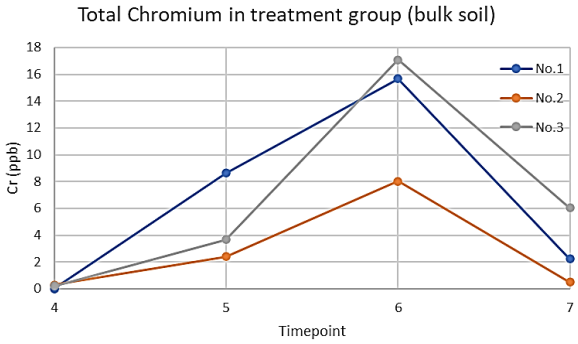

Figure 23. Total measured Chromium of the treatment group with oxalic acid addition over four distinct sampling points (bulk soil)

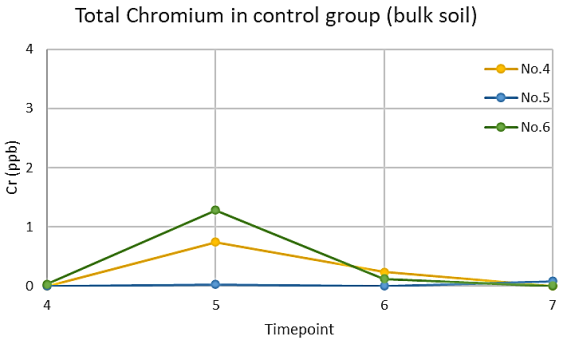

Figure 24. Total measured Chromium of the control group over four distinct sampling points (bulk soil)

Oxalic acid addition: Effect of pH, Eh and OM on Chromium bioavailability and speciation

Analysing the monitored pH during the experiment, it becomes clear that pot Nr.2 and 3 of the treatment group remained fairly stable for most points around 5-5.5, whereas pot Nr.1 experienced an extreme pH drop to a value of 3.5, as shown in Figure 25. Studies show that rice plants prefer a pH range between 5.0 and 6.5 in order to thrive[69]. Also, by looking at the nutrient availability at different pH ranges, we see that below a pH of 4.5, most plants experience a nutrient deficiency, as almost all of the microelements, such as nitrogen and phosphorus, are not bioavailable anymore[70]. Furthermore, at such an extremely acidic pH, the Cr(III) dissolution could be driven mainly by the proton and not the ligand[21]. What caused the pH drop in only one pot but not the other experimental units remains unclear. Regarding the control group (Figure 26), all three pots also experienced a decreasing tendency of the pH, but not below 4.5. This can be explained by either the exudation of rice root exudates that have the ability to alter the soil pH or with continuous weathering and leaching of soil minerals[71] [72].

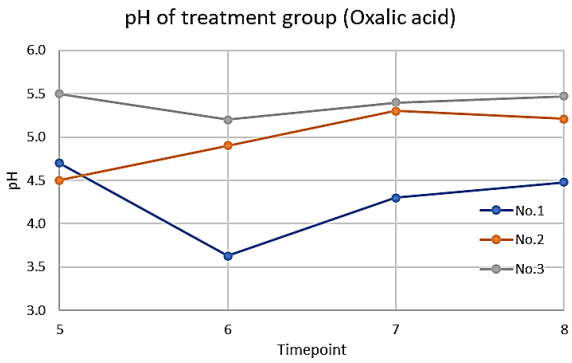

Figure 25. Measured pH values of the treatment group with oxalic acid addition over four distinct sampling points

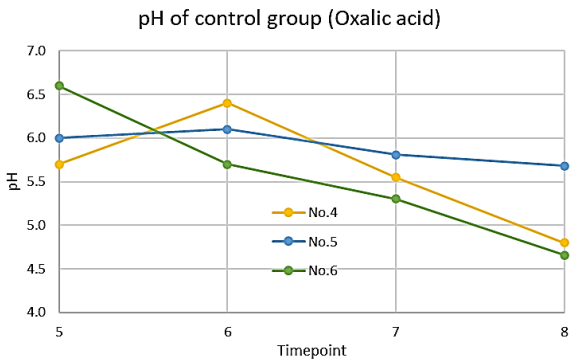

Figure 26. Measured pH values of the control group over four distinct sampling points

Examining the redox conditions of the paddy system from the treatment group (Figure 27), a similar trend for all pots can be observed. After the addition of oxalic acid, the Eh values increased drastically from -200 mV / -300 mV to values between 0 and +250 mV, meaning that the conditions changed from reducing to oxidizing within a very short period of time. An explanation for this occurrence could be that the aerated roots of the rice plants provided a pathway for O_2 diffusion within the rhizosphere. This mechanism of internal aeration was found in plants that grow in water-logged soil, like *Oryza sativa*[73]. An alternative explanation for the elevated Eh values is the release of other cations from the soil to porewater caused by the addition of oxalic acid. In suboxic environments (350mV > Eh > 100mV), the pH is the crucial factor deciding the Cr speciation[21]. Under a pH of 6, which was observed in this system, the dominant species would still be Cr(III). The redox potential of the control group's system, as seen in Figure 28, remained stable between -100mV and -250mV.

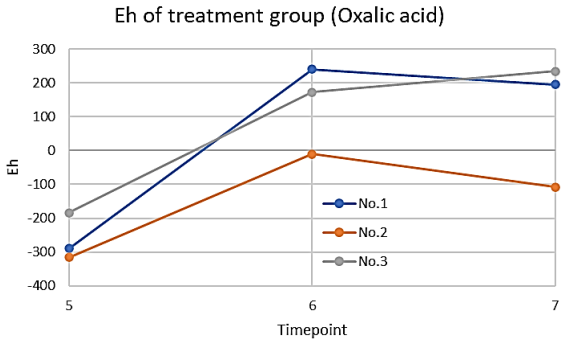

Figure 27. Measured Eh of the treatment group with oxalic acid addition over three distinct sampling points

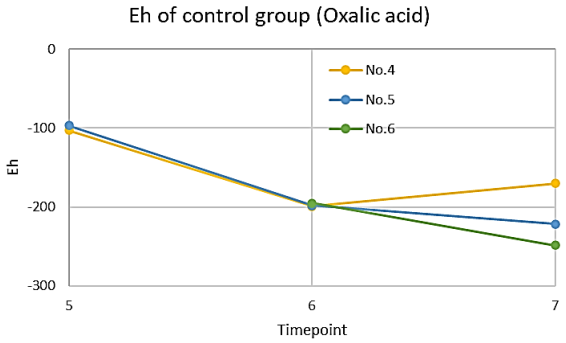

Figure 28. Measured Eh of control over three distinct sampling points

Cr-Fe-Mn redox interplay

The redox interplay among iron, manganese and chromium is a dynamic and crucial aspect of our paddy system. Here, iron plays a role as an adsorption and reduction agent for Cr. Under reducing conditions, such as in waterlogged soils or flooded environments, Fe(III) can be reduced to Fe(II) by microbial activities. The reduced iron speciation includes aqueous Fe^0, Fe(II), Fe(II) hydroxides and Fe(II) chelates[21]. Cr(VI) can rapidly be reduced by Fe(II) to subsequently form Cr(III)-Fe(III) hydroxides with a low solubility. These ferrous compounds are the most common reductants of Cr(VI) in nature[74]. In the process of Cr(VI) adsorption and reduction, the newly generated Cr(III) binds to the hydroxyl groups present on the surface of Fe oxides, creating an inner-sphere bidentate surface complex[75]. Manganese similarly exhibits redox cycling between Mn(II) and Mn(IV) states. In anaerobic environments, manganese reduction leads to the formation of soluble Mn(II), while aerobic conditions favour manganese oxidation to form less soluble Mn(IV) oxides. Mn oxides can oxidize Cr(III) and promote the release of Cr[76]. In terms of thermodynamics, natural oxidants that can oxidize Cr(III) are limited to Mn oxides and oxygen, but their oxidation rates differ. Because of the slow reaction kinetics, the oxidation rate of Cr(III) by dissolved oxygen is extremely slow under natural conditions[77]. A number of experiments confirmed that active Mn(IV) oxides can promote Cr(III) oxidation significantly greater than O_2 alone under low oxygen conditions[78]. In order to compare the Cr, Mn and Fe values in our system, the results were plotted for each element (average value) over the whole course of the experiment, where the time points 0-4 are with DFOB addition and the timepoints 4-8 are with the addition of oxalic acid. As already discussed in the section above, the Cr concentrations taken from the pore water only spike after the treatment with oxalic acid, as shown in Figure 29. Analysis of dissolved Fe concentrations showed two distinct peaks, as depicted in Figure 30. The first increase in soluble Fe can be observed after the addition of DFOB at timepoint one. This can be explained by the acidic pH and the reducing environmental conditions of the system during that timepoint, but is also consistent with the ligand induced dissolution of Fe in the system. As demonstrated in previous studies, in the presence of the siderophore DFOB, iron can be released to a great extent from solid phases[79]. The second Fe peak is in the middle of the oxalic acid treatment stage. The values of the second peak are 3.5× larger than with the DFOB present. This may be because the molarity of oxalic acid was 100 times higher than DFOB. Generally, oxalic acid efficiently dissolves Fe oxides under various conditions due to its high acid strength, reducing properties and complexing ability[80]. As we also observed exactly the same peaks (but a few orders of magnitudes lower) in the control group, other factors like the pH, Eh and OM content of the soil system must also contribute to the dissolution of Fe from the soil, in addition to organic ligands. By analysing the speciation of Fe using the ferrozine method on the plate reader, we found that both Fe(II) and Fe(III) are present in the system. No clear trend could be observed setting the treatment group and the control group side by side. Comparing the Mn concentrations (Figure 31) to the Fe, it becomes evident that soluble Mn exhibits only one maximum around the seventh time point. This shows that DFOB does not drive Mn dissolution, but oxalic acid has the ability to do so. According to

Wang et al., 2006 the dissolution of Mn can be due to reductive dissolution with the possibility of ligand-assisted dissolution in the case of oxalic acid. This finding is supported by the fact that the control group also showed slightly higher Mn in solution values around the same time point. Besides, lowering the soil pH may also result in an increased level of Mn in the porewater of the paddy system due to proton-promoted dissolution[82].

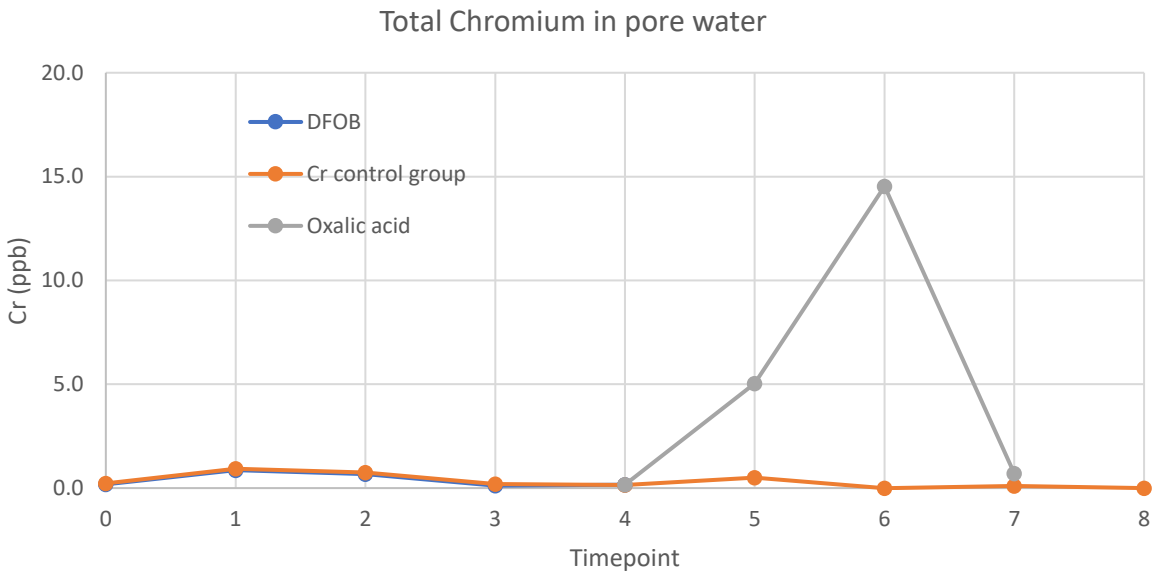

Figure 29. Measured Chromium values over the duration of the entire experiment with the addition of DFOB (timepoints 0-4) and oxalic acid (time points 4-8) for the treatment group and the control group values

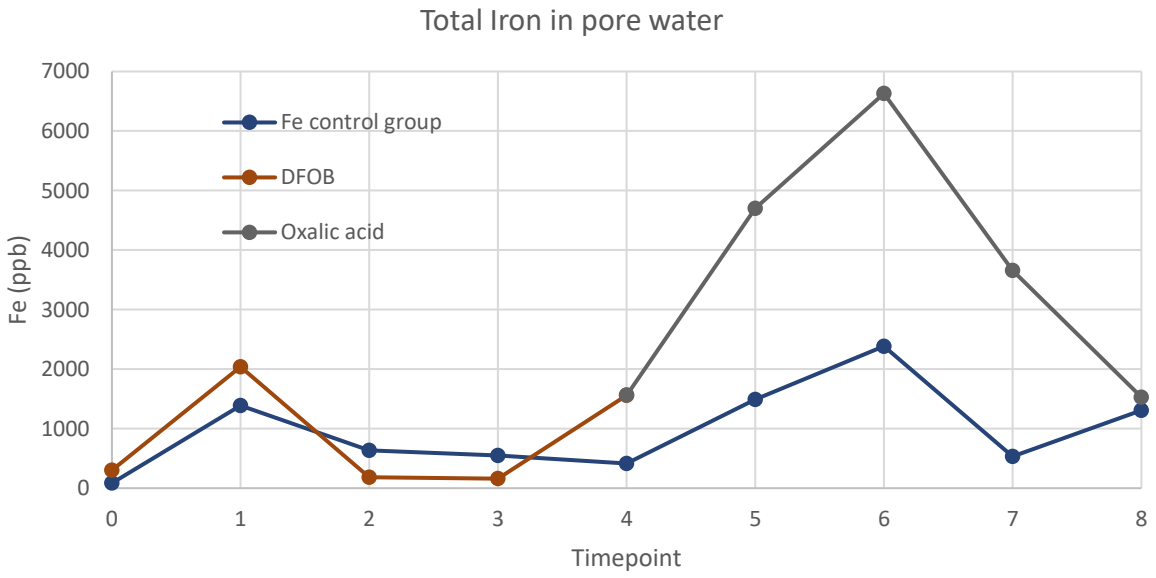

Figure 30. Measured Iron values over the duration of the entire experiment with the addition of DFOB (timepoints 0-4) and oxalic acid (time points 4-8) for the treatment group and the control group values

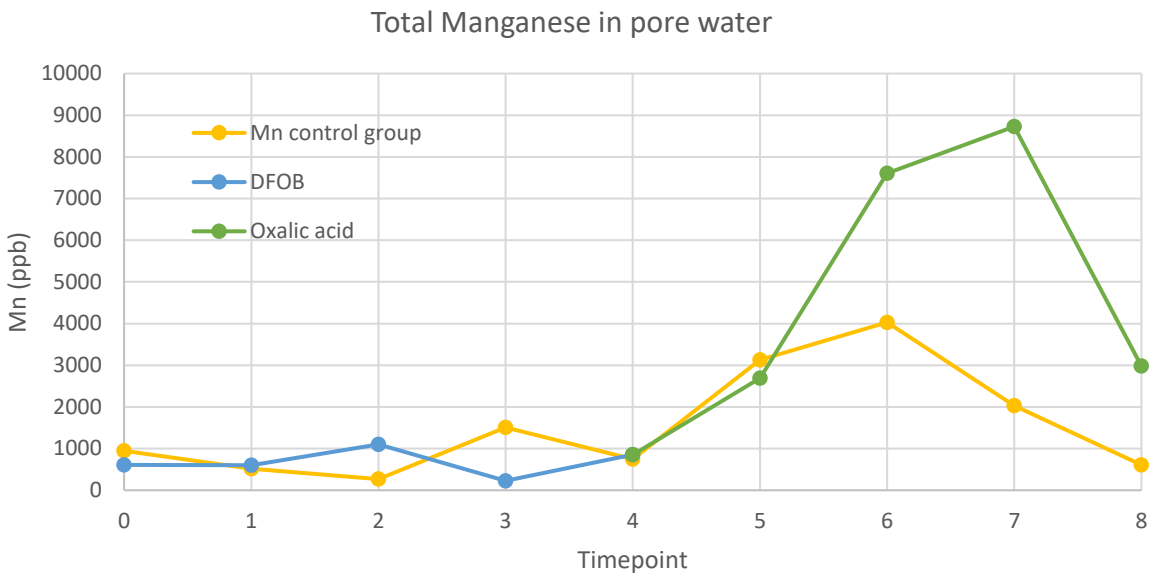

Figure 31.Measured Manganese values over the duration of the entire experiment with the addition of DFOB (time points 0-4) and oxalic acid (time points 4-8) for the treatment group and the control group values

In summary, the paddy soil system is a very complex environment with multiple factors influencing the behaviour of Cr via different processes (e.g., redox dependent vs. independent). This makes it extremely difficult to determine which factor is the driving force or to understand the interplay between different components. In order to gain a better understanding of this, so called black-box-system another experiment was designed. Here, the focus was on breaking down this multi-factorial environment and studying these processes separately on a smaller scale.

Microfluidic reactor design and method development

The final angle of this master project encompasses an approach towards pore-scale contaminant biogeochemistry. The aim was to develop a mineral-embedded "soil-on-a-chip" model to study the previously discussed processes under the microscope. Three different techniques were used to build three different models. The first method used a regular microfluidic reactor made from resin that was coated with minerals (Picture 1). The second one embedded the minerals directly into the polydimethylsiloxane (PDMS) of the reactor (Picture 2), and the last one used a regular PDMS microfluidic reactor, pumping the minerals in suspension into the pore space (Picture 3). In this section, the different types of newly fabricated microfluidic devices are compared and rated for further development and use.

Picture 1. Resin-based microfluidic reactor coated with Cr-mineral

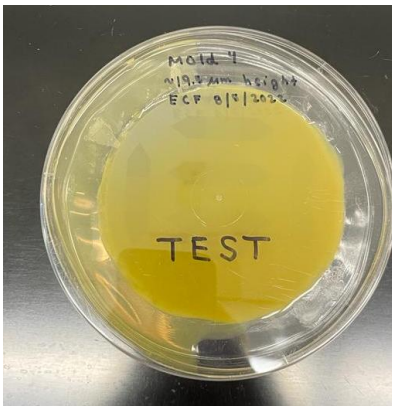

Picture 2. PDMS-based microfluidic reactor embedded with Fe-mineral

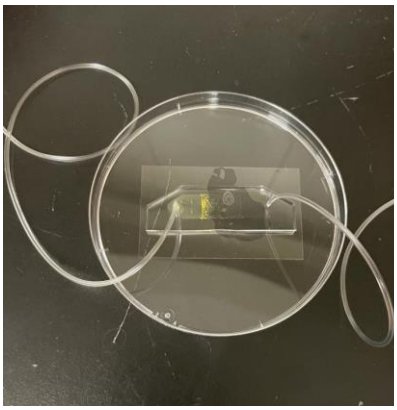

Picture 3. PDMS-based microfluidic reactor flooded with Fe-mineral suspension

All three approaches were analysed regarding their general functionality and usability for further laboratory experiments and the extent of minerals that were incorporated and accessible in the reactor. This analysis was mainly focused on the accessible part of the reactor, the pore space, as this is the most relevant part of the reactor in terms of environmental implications. Therefore, the percentage of the grains (41%) was calculated and subtracted from the total image, resulting in the percentage of the pore space (59%). This percentage was used for further quantification.

Resin-based microfluidic reactor coated with Cr-mineral

Evaluating the first newly designed reactor, it becomes apparent that the mineral that was sprayed onto the device spread unevenly, forming a very densely coated area on the pore space edges and a low mineral area in the middle of the pore space (Picture 4). Furthermore, the mineral deposition was attributed mostly on the glass bottom and on top of the grains, contrary to the intended coating of the edges of the gains. This shows that it is extremely difficult to coat all the accessible parts of the reactor evenly. Additionally, it can be assumed that recreating this reactor would lead to a different distribution of minerals, making an exact replication impossible. Using MATLAB to analyse the extent of the Cr mineral coverage inside the pore space, we see that 43.7% of the accessible pore space is covered in Cr

minerals. The coverage percentage, in general, is satisfactory and could indicate successful experiments with this model, but the distribution is not conducive to consistent or reproducible experiments. This approach could be adapted to the field of Millifluidic reactor fabrication[83]. Here the reactors are larger, and the pore space could be spray coated more precisely and evenly.

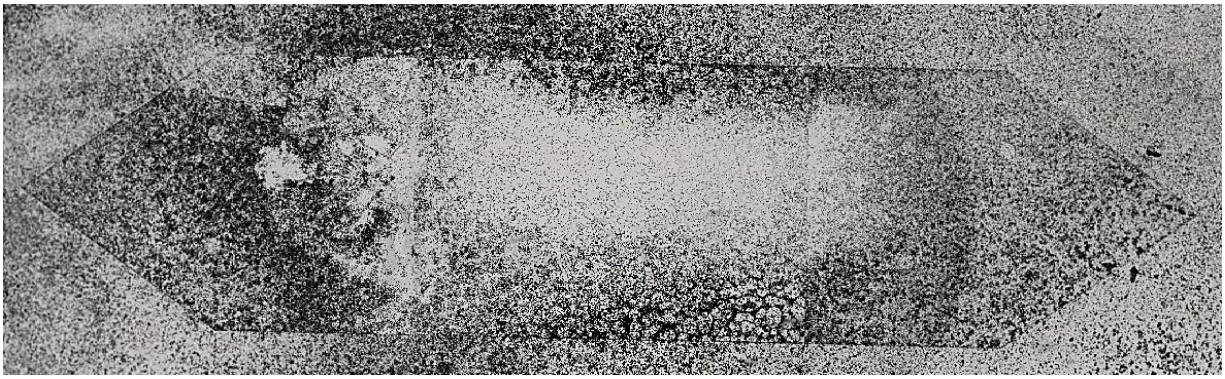

Picture 4. Resin-based microfluidic device, mineral distribution (microscopic, stitched image; 4x)

Another notable issue with this reactor design is cracks in the pore space that develop as the ethanol-mineral suspension dried, which creates a nonuniform surface within the microfluidic reactor (Picture 5). Lastly, the main problem that became unavoidable was that the reactor could not be sealed water-tight for further experiments. The resin reactor could not be plasma bonded to the PDMS as the surfaces are too rough to allow a tight seal to form. Using PDMS and a sticky form of PDMS (not fully cured substance), no closed reactor could be achieved. Unfortunately, this design was abandoned since it was not easily reproducible, and no further flow-through experiments could be conducted, as the design does not work for continuous flow studies or experiments involving bacteria. Alternatively, this reactor design would be suitable for experiments where no saturated conditions are required, f.e. grow fungi or similar colonies in it and study different growth traits under the microscope[84].

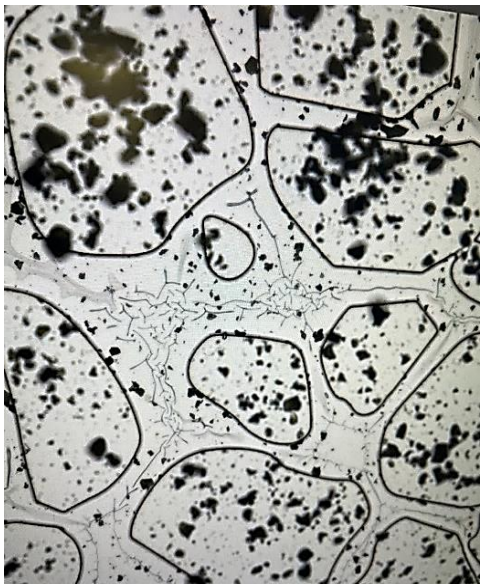

Picture 5. Resin-based microfluidic device, pore space detail with cracks (microscopic image; 10x)

PDMS-based microfluidic reactor embedded with mineral

The second approach was inspired by the first design and the study conducted by Bhattacharjee et al. 2021. The authors created a PDMS reactor that contained minerals by directly mixing kaolinite powder with the liquid PDMS. After mixing the components, they allowed the mineral to sediment overnight[85]. We adapted this approach for our experiment by mixing Fe or Cr oxide powder into the liquid PDMS and then curing as described in the methods above. In the following section, we assess the functionality of the two reactors.

In the Fe-infused PDMS reactor, we observed that the fine goethite powder (average particle size between 0.1 – 1 µm [86]) mixed extremely well with the PDMS and was distributed evenly. This experiment was inspired by the previous study by Huang et al., 2012. They successfully introduced an Fe(III)-oxide nanoparticle/PDMS composite into one of their reactors. They found that the Fe mineral, when mixed into the PDMS, is enveloped by the entangling polymer chains, ensuring a well-mixed composite[87]. This led to a bright yellow colouration of the PDMS film, as shown in Picture 6. In order to further analyse the reactor and quantify the amount of Fe mineral that was accessible inside the reactor pore space, the device was imaged using a Nikon microscope with a 4x magnification. To gather a large image of the entire reactor, smaller images are taken and stitched together (1% overlap). This process turned out to be quite difficult with the heavily colourised microfluidic reactor, as shown in image 7.

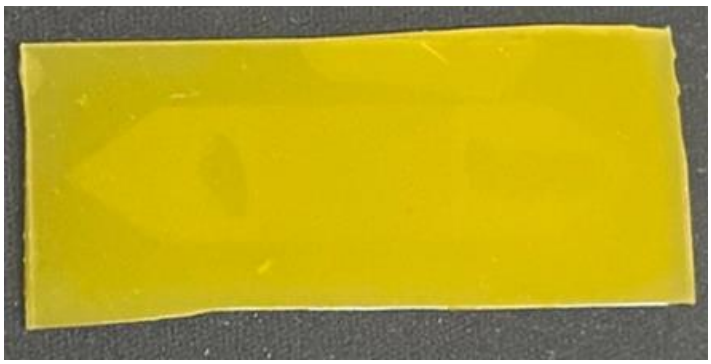

Picture 6. PDMS-based microfluidic reactor mixed with goethite powder

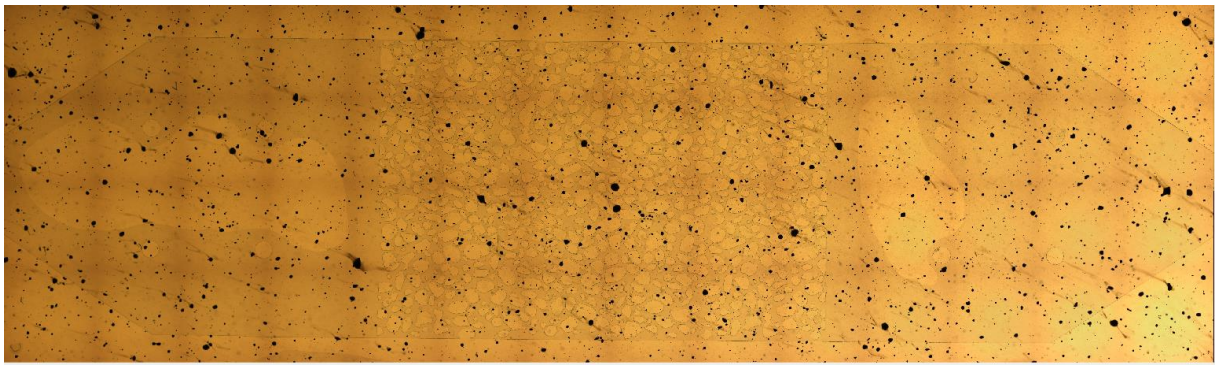

Picture 7. PDMS-based microfluidic device mixed with goethite powder (microscopic, stitched image; 4x)

The coloration increased the opacity of the PDMS, therefore changing the illumination time required to capture the image, and ultimately failing to generate a raster-free image. This problem proved to be quite serious as the MATLAB analysis that was used to quantify the mineral amount segments the image according to the coloration. This function converts the grayscale image to a binary image by replacing every pixel in the first image with a luminance greater than a chosen level with the value 1 (white) and replacing all other pixels with the value 0 to black[88]. Ultimately distorting the results of the mineral quantity in the reactor pore space. Specifically, this leads to an underestimation of the mineral quantity in the reactor pore space. Generally, the results are extremely hard to quantify as it is unknown of how accessible the incorporated Fe is. Using the same MATLAB script as previously described, the mineral aggregates were isolated and quantified, as depicted in Picture 8. This analysis showed that 10.1% of the accessible pore space is covered with Fe-aggregates in the PDMS. But as the rest of the well mixed Fe remains unquantifiable, these results are not satisfactory. Additionally, no data on the amount of

added Fe that is aggregated versus mixed into the PDMS could be obtained. Lastly, no information was generated on how much Fe is available to react with fluids at the grain surface.

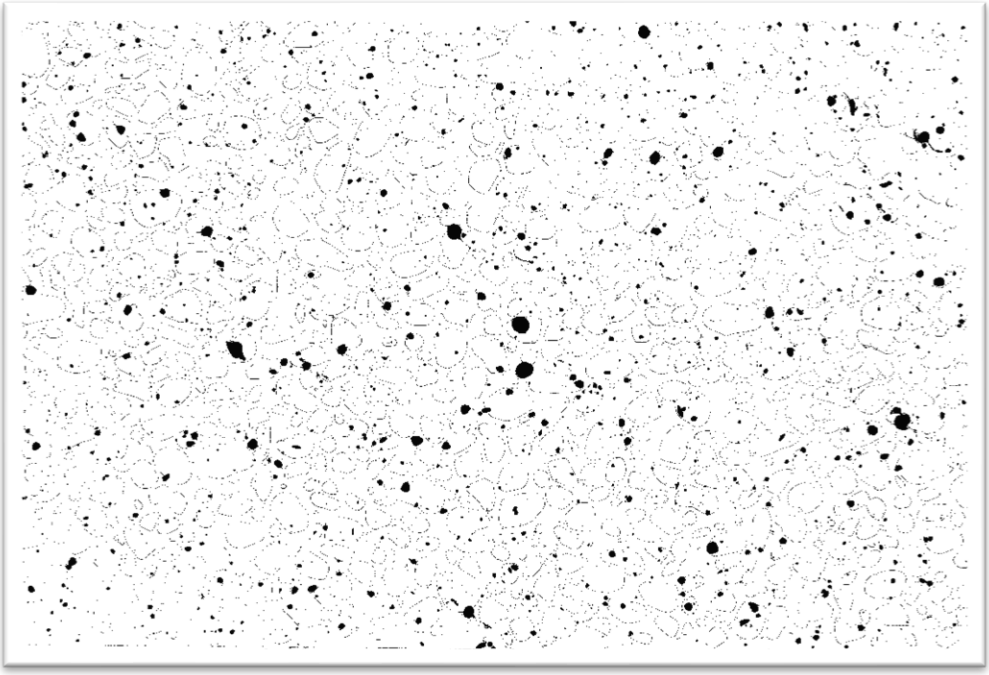

Picture 8. Cropped, threshold-applied image of the PDMS-based reactor mixed with Iron mineral (4x), Image analysis performed in ImageJ.

Moving on to the PDMS reactor mixed with Cr mineral, we encountered the opposite outcome as for the goethite/PDMS test. Independently on how the Cr(III) was added (liquid or powder form), no full Cr and PDMS mixture could be achieved. For example, the liquid $Cr(OH)_3$ remained a single droplet encompassed by the liquid PDMS. After vigorous stirring, the droplet separated into smaller droplets, but PDMS and Cr remained immiscible, so no mixing was observed. This can be explained by the relatively low solubility of Chromium hydroxide ($k_{sp}= 6.7x10^{-3}$)[89]. Additional factors that could support the immiscibility might be the hydrophobic nature and the negative surface charge of PDMS. After pouring the liquid PDMS into the mould and letting it cure, the pore space remained without visible $Cr(OH)_3$ aggregates. Therefore, no MATLAB quantification was conducted.

PDMS-based microfluidic reactor pore space flooding with mineral suspension

The last approach was based on the study conducted by Alzahid et al., 2018. They tested the functionalisation abilities of PDMS by introducing mineral mixtures (Sandstone and Carbonate mixtures) to the microfluidic device. After treating the PDMS with oxygen plasma, they discovered that the silicate oxygen groups in the quartz, kaolinite, and hydrogen groups along the edge of the kaolinite particles bond with the silanol groups on the PDMS surface[90]. Following exposure to the oxygen plasma, silanol groups (Si-OH) replace the $-CH_3$ on the Polydimethylsiloxane structure. Prior to the oxygen plasma exposure, PDMS was comprised of $O\text{-}Si\text{-}(CH_3)_2$ units. Afterwards, the Si-OH groups can bond with other functional groups[90]. For our experiment, a regular PDMS-based reactor was fabricated and

fully set up for a flow-through study. This included punching holes for the inlet and outlet, plasma bonding the reactor shut, and connecting tubing. The outlet tubing was further connected to an effluent collection vial for analysis, and the inlet tubing to a syringe attached to a syringe pump (NE-4002X programmable microfluidic syringe pump, New Era). The syringe was loaded with either $Cr(OH)_3$ suspension, which was previously centrifuged to sort out larger, tube-clogging particles or an aqueous suspension of goethite. Both suspensions were injected at a flow rate of 1ml/h with a total volume of 1ml. The particle size that was aimed to avoid tube clogging was smaller than 0.5mm in diameter, as this was the inner diameter of the tubing.

Analysing the first controlled injection of 0.1 M Chromium hydroxide into the reactor pore space, we observe that 13.95% of the accessible pore space is covered with Cr-minerals, as shown in Picture 9. The mineral particles settled along a straight path from the inlet (left hole) into the reactor pore space. Here, they are mainly distributed in the middle part of the reactor.

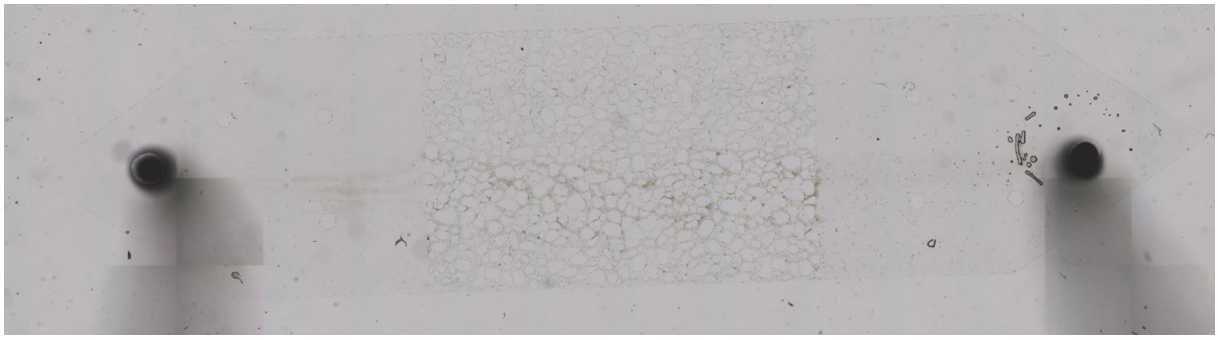

Picture 9. PDMS-based microfluidic reactor after the injection of 0.1 M $Cr(OH)_3$ suspension at a flow rate of 1ml/h; Showing a path of retained mineral from the inlet (left hole) into the reactor pore space (4x).

Picture 10. PDMS-based microfluidic reactor after the injection of 0.1 M $Cr(OH)_3$ suspension at a flow rate of 1 ml/h and after flushing through 1 ml MilliQ water at 1ml/h; Showing retained mineral well distributed inside the reactor pore space (4x).

In order to test the mineral's physical resistance to applied fluid flow inside the reactor, MilliQ water was injected using the same parameters as before (Picture 10). The MilliQ flush is performed to gain insides on how well the introduced mineral remains inside the reactor. So, if the mineral flushes out quickly after injecting MilliQ water, a low physical resistance of the mineral inside the reactor is assumed. On the contrary, if the mineral remains stationary inside the reactor pore space, a high physical resistance is assumed. Using the MATLAB script, the pore space data showed that 13.33% was still

covered with Cr-mineral. This means that 0.6% of the previously mineral covered pore space is now without particles. This equals approx. 4% of the mineral that was washed out during that step. To support these image analysis data, the effluent from all injections was collected and analysed with ICP-MS. The results are shown in Figure 32.

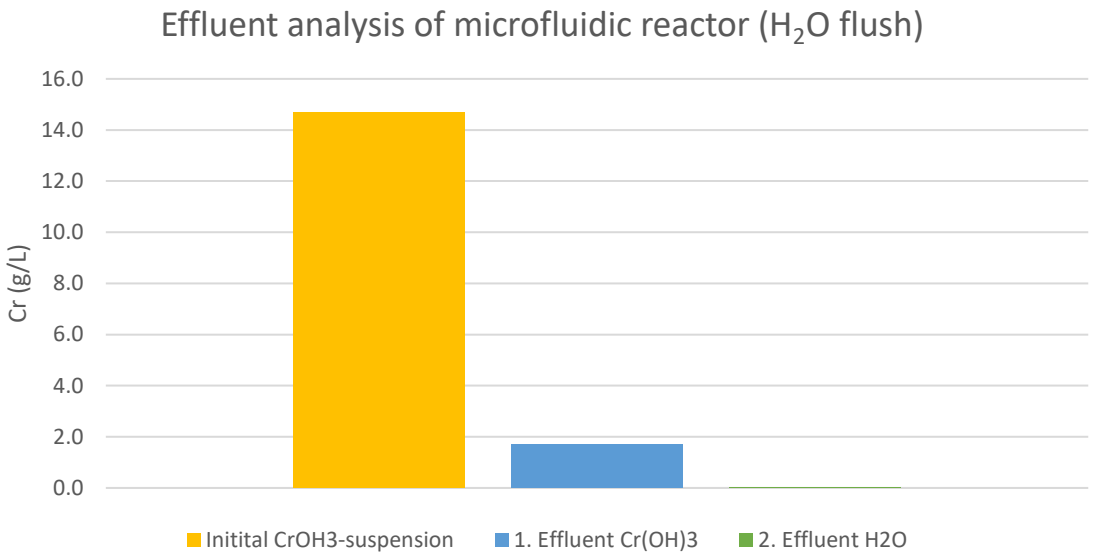

Figure 32. ICP-MS results of the collected effluents (g/L). First effluent (blue) was collected while injecting the Chromium hydroxide suspension. The second effluent (green) was collected while injecting the MilliQ water. Effluent data is compared to the initially prepared $Cr(OH)_3$ suspension (yellow).

Comparing the initial $Cr(OH)_3$ suspension (0.1M) to the collected first effluent, we can assume that, as only 1.72 g/L were in the effluent vial, 88.3% of the mineral remained inside the reactor pore space. After flushing the microfluidic device with water, only 0.01 g/L was detected in the second effluent. This means that 88.2% of the mineral is still inside the reactor. From this analysis, we can conclude that less than 1% of the mineral is washed out. However, it should be considered that some of the Cr particles could still be inside the tip of the syringe or even the tubing, which would alter the results. For follow-up studies, it would also be recommended to account for that by closely inspecting the described parts. Generally, we can conclude that the mineral is stable enough to withstand flushing the reactor with water.

This study went one step further and additionally tested the physical resistance of the mineral by flushing through a strong oxidizing agent of Cr, Manganese Pyrophosphate (Mn-PP). Similar to the first experiment, a $Cr(OH)_3$ suspension was injected into the rector. This time, the concentration of the initial Cr suspension was 0.05 M, but the flow rate and volume remained the same. The microscopic result of the mineral injection is depicted in Picture 11. Using MATLAB, we calculated that 14.75% of the accessible pore space is covered with Cr mineral. This value is similar to the previous experiment, where 13.95% were covered. The second step involved the introduction of 100 µM Mn-PP into the reactor, a powerful oxidizing agent of Cr. After this flush, 12.88% of the accessible pore space is covered with Cr-mineral, meaning a loss of 1.88% of covered pore space (Picture 12). This translates to 13% of the

introduced mineral being dissolved and washed out during the Mn-PP flush. Comparing this value to the previous physical resistance test using water, we see that the percentage of lost minerals is 3x higher flushing with the oxidizing agent than with water. Previous studies on the interaction of Mn-PP and Cr(III) show that Mn(III) can effectively oxidize Cr(III) to Cr(VI) and that a significant amount of Cr(VI) is released into the aqueous phase[91]. But, as we analysed, not all of the Cr(III) is oxidized and solubilized. This is due to the fact that Cr(VI) can adsorb back onto the Chromium hydroxide surface[91].

Picture 11. PDMS-based microfluidic reactor after the injection of 0.05 M $Cr(OH)_3$ suspension at a flow rate of 1 ml/h; Showing a cluster of retained mineral from the inlet (left hole) into the upper left corner of the reactor pore space (4x).

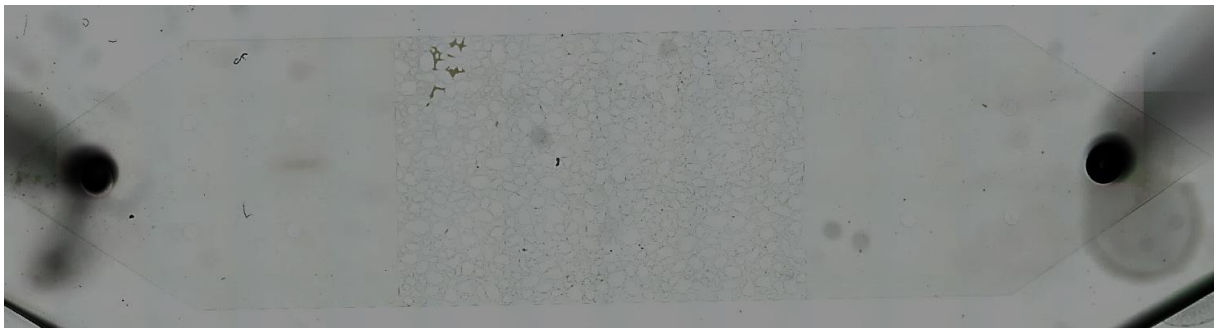

Picture 12. PDMS-based microfluidic reactor after the injection of 0.05 M $Cr(OH)_3$ suspension at a flow rate of 1ml/h and after flushing through 1 ml of 100 µM Mn-PP at 1ml/h; Showing remaining mineral inside the reactor pore space (4x).

The effluent of the second experiment was analysed, as shown in Figure 33. Comparing the initial suspension to the first effluent, we can deduce that 86.1% of the Cr(III) remained inside the reactor. Again, unfortunately, the syringe tip and tubing could not be accounted for, and this study can only acknowledge that there is a possibility of minerals still remaining in those parts of the set-up. After the Mn-PP flush, the mineral that is still inside the reactor came up to 85.3%. This would mean a mineral loss of less than 1% during this experiment.

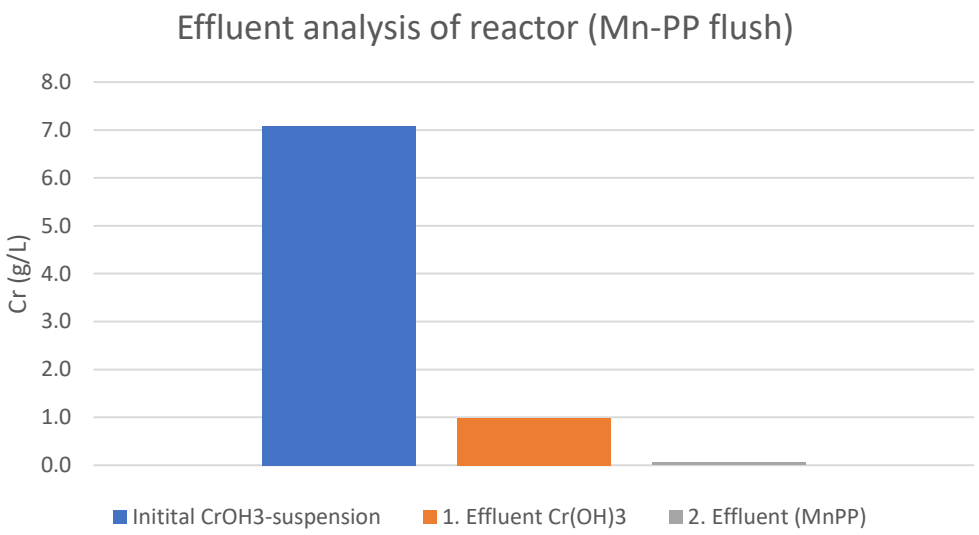

Figure 33. ICP-MS results of the collected effluents (g/L). First effluent (orange) was collected while injecting the Chromium hydroxide suspension. The second effluent (grey) was collected while injecting the Mn-PP. Effluent data is compared to the initially prepared $Cr(OH)_3$ suspension (blue).

To clarify, using the MATLAB image analysis, we focus on the accessible part of the reactor, the pore space, and by analysing the effluent, we only see what is washed out of the entire reactor. So, if these values do not match up, it could mean that the mineral is already washed out of the pore space but might still be inside the reactor or the outlet tubing. In conclusion, we can clearly see that the physical resistance of the mineral can withstand the water flush, but the Mn-PP has the ability to mobilize a significant part of the Cr(III). This means that this design can be used for certain follow-up experiments but not as a general omni-usable microfluidic reactor. As this experiment still seemed quite successful, the same method was tested for an Iron-suspension. The aqueous goethite suspension (0.1 mM) was injected at a flow rate of 1ml/h with a total volume of 1ml. The results are shown in Picture 13. Using the image analysis software, it shows that 13.3% of the accessible pore space is covered with Fe-mineral, which is again in the same range as the previous experiments.

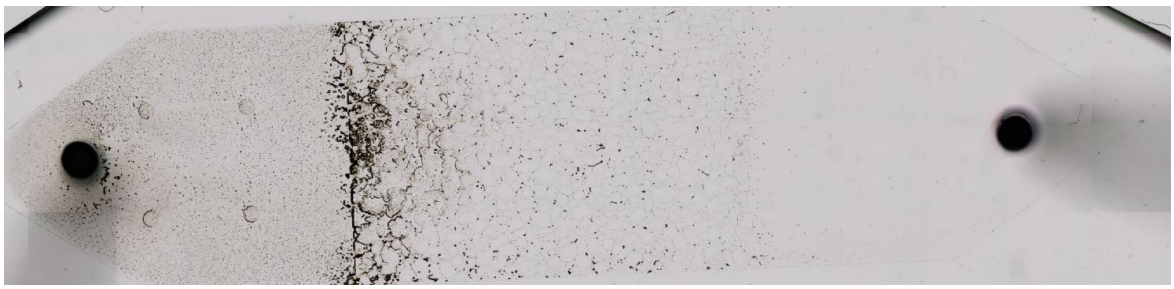

Picture 13. PDMS-based microfluidic reactor after the injection of 0.1 mM Fe(III) suspension at a flow rate of 1 ml/h; Showing a cluster of retained mineral from the inlet (left hole) of the reactor pore space to the front line of the pores (4x).

Seeing that the mineral was deposited inside the reactor, the next step was to test the physical resistance of the Fe-mineral inside the pore space. For this purpose, oxalic acid, a reducing agent, was added first,

followed by the chelating agent EDTA. These two ligands were chosen because of their dissimilar characteristics. With oxalic acid we assume that it dissolves the Fe oxides, making them soluble and more likely to wash out of the reactor[80]. By adding the EDTA, we presume that the chelating agent forms Ferric EDTA with the Iron, remaining inside the reactor[92]. Unfortunately, due to unknown circumstances, the oxalic acid injection led to the unsealing of the reactor. Reasons for this could be a reaction of PDMS with either EDTA or oxalic acid or the reactor was not sealed completely during the plasma treatment. This resulted in most of the minerals sticking to the bottom of the grains and air bubbles being introduced into the system. The result of this is shown in Picture 14. No further investigation was conducted.

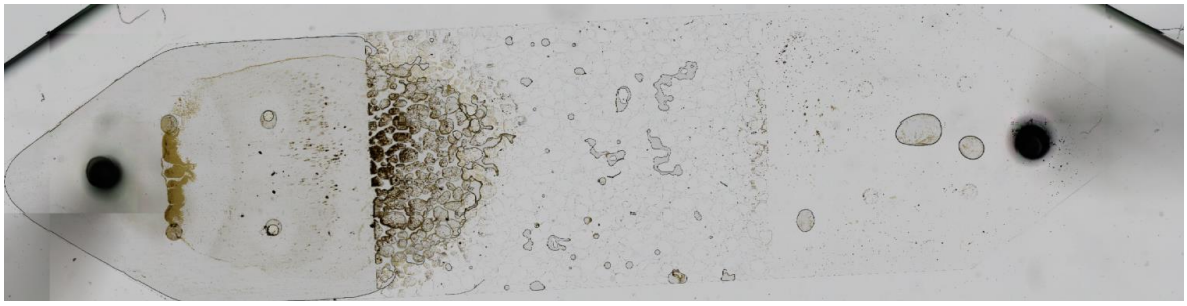

Picture 14. PDMS-based microfluidic reactor after the injection of 0.1 M oxalic acid at a flow rate of 1ml/h; Showing the Fe-mineral sticking to the bottom of the grains and air bubbles inside the reactor (4x).

Conclusion

Summing up the individual chapters, firstly, the paddy soil material from Sukinda Valley (India) was characterised, together with mineral composition determination that shows the soil is rich in silicates. Following sequential and total extraction protocols, the elemental composition was determined, showing high levels of heavy metal contents and Cr contamination, which is due to an active chromite mine in the study area. Secondly, a batch soil leaching experiment was conducted. Ligand induced Cr dissolution from the model compound Chromium(III) hydroxide and from the soil sample was evidenced when different types of organic ligands at different concentrations were utilised. It was found that all ligands tested (DFOB, citric acid, and oxalic acid) caused higher levels of dissolved Cr concentrations compared to the control group. Citric acid could greatly induce $Cr(OH)_3$ dissolution, whereas DFOB showed less significant effects. Results from the pot experiments showed oxalic acid induced Cr dissolution in the plant-soil system, whereas DFOB did not show significant effects. Additionally, the effects of pH, Eh, and organic matter content on Cr cycling in this system were discussed; the complex redox interplay between iron, manganese and chromium was also investigated. It is difficult to pinpoint what effects were the driving or limiting factor in the Cr cycling with existing data, but another experiment was designed to piece together multiple processes. In order to solve the mystery of the so-called black box that represents the soil, a microfluidic reactor design was developed. The purpose was to integrate a reactive surface into the microfluidic device to analyse biogeochemical processes under the microscope. To achieve this, several steps were taken, including experimenting with the material of the reactor and the introduction of minerals into/onto the device. To conclude, in this study, the biogeochemistry of chromium was explored over various time points at multiple scales: from micro (soil-on-a-chip) to milli (batch experiment) to macro (pot experiment). Results from this study provide new insights as to the role of organic ligands in the Cr(III)-Cr(VI) redox cycle and are valuable for future studies that quantify the behaviour of Cr in a system where multiple processes can occur.

Limitation

Regarding the limitations of this master thesis, there are a few things that should be noted. Firstly, the rice was not given sufficient nutrients or fertilizer solution once the experiment had started. This caused a lack of macronutrients for the rice plants to grow. However, due to the possible interference with the ligand treatment, there was a decision against a fertilization step during the study. Additionally, one more control experiment could have been added to the design, i.e. a pot with soil only (without plants), but the addition of the ligand was done in the same way as the other groups. This could help distinguish the role of natural organic acid exudation or the aerating roots from the rice plants. However, this would require significantly larger amounts of soil materials that are shipped from the sampling sites. Nevertheless, this project provides first-hand information on designing laboratory-controlled experiments to investigate metal biogeochemical cycling at different scales, based on which further studies will build up.

Environmental Importance

This study utilised combined experimental approaches to highlight that ligand induced Cr dissolution in Cr contaminated paddy fields can occur. This process has important environmental implications because as the ligand forms complexes with chromium in soil, the solubility, mobility and, ultimately the bioavailability can change. In our case, the enhanced solubility can potentially lead to increased mobility, allowing the element to be transported over greater distances. This has implications for the pollution mitigation of surface water, pore water and groundwater[93]. Furthermore, the complexed forms of chromium may be more readily taken up by organisms, influencing their exposure and potential for bioaccumulation. Mishra et al. (1997) showed that Cr(III) and Cr(VI) can both be taken up by the rice roots and accumulate in plants. Cr additionally negatively impacts plant growth by disrupting their essential metabolic processes. This toxic effect is related to the formation of reactive oxygen species (ROS), leading to oxidative stress[95]. Another factor that plays an important role in the redox cycling and transformation of Cr in soil. Multiple factors such as pH, Eh and the presence of Fe and Mn in the system, in addition to organic ligands, can dictate the speciation of Cr. Cr(VI) is known to be more mobile and more toxic than Cr(III). Furthermore, chromium contamination in paddy soils can have adverse effects on soil health, affecting the physical, chemical, and biological properties of the soil. This can lead to decreased soil fertility and productivity[96].

From a human perspective, not only consuming rice grown in chromium-contaminated soil but also planting and harvesting it may expose humans to elevated levels of Cr. This might result in adverse health effects; for example, chronic exposure to high levels of hexavalent chromium has been associated with respiratory issues, skin irritation, and an increased risk of certain cancers[97]. Governments and environmental agencies set regulatory limits for chromium concentrations in soils and water to protect human health and the environment[98]. Studying chromium in paddy soils helps assess compliance with these regulations and implementing effective remediation strategies when necessary. Regarding the sampling site in the Sukinda Valley, it becomes apparent that the recommended Cr levels are by far exceeded. In order to help with pollution mitigation, a different approach on how to mine chromite must be developed in combination with environmental remediation. Here, knowledge about the behaviour of Cr in paddy soils is crucial for developing an effective remediation strategy. Various techniques can be targeted, such as phytoremediation, microbial remediation, and soil amendments to mitigate Cr contamination and restore the health of the affected soil[96]. These measures are essential to decrease the ecological threat of chromium.

References

(1) Walsh, B. The world's most polluted places. *Time Magazine* **2007**, 1-3.
(2) Nriagu, J. O.; Nieboer, E. *Chromium in the natural and human environments*; John Wiley & Sons, 1988.
(3) Oze, C.; Bird, D. K.; Fendorf, S. Genesis of hexavalent chromium from natural sources in soil and groundwater. *Proceedings of the National Academy of Sciences* **2007**, *104* (16), 6544-6549.
(4) Ma, Y.; Hooda, P. S. Chromium, nickel and cobalt. *Trace elements in soils* **2010**, 461-479.
(5) Díez, M.; Simón, M.; Martín, F.; Dorronsoro, C.; García, I.; Van Gestel, C. Ambient trace element background concentrations in soils and their use in risk assessment. *Science of the Total Environment* **2009**, *407* (16), 4622-4632.
(6) Emsley, J. *Nature's building blocks: an AZ guide to the elements*; Oxford University Press, 2011.
(7) *Chromium Market Outlook Report By Application (Metallurgy, Chemicals, Refractory), By Region (North America, Europe, Asia Pacific, Central & South America, Middle East & Africa), And Segment Forecasts, 2020 - 2025*; Grand View Research, Grand View Research, 2019. https://www.grandviewresearch.com/industry-analysis/chromium-market.
(8) *Mineral commodity summaries 2023*; National Minerals Information Center, 2023. DOI: 10.3133/mcs2023.
(9) Das, S.; Ram, S.; Sahu, H.; Rao, D.; Chakraborty, A.; Sudarshan, M.; Thatoi, H. A study on soil physico-chemical, microbial and metal content in Sukinda chromite mine of Odisha, India. *Environmental earth sciences* **2013**, *69*, 2487-2497.
(10) Nayak, S.; Kale, P. A review of chromite mining in Sukinda Valley of India: impact and potential remediation measures. *International Journal of Phytoremediation* **2020**, *22* (8), 804-818.
(11) Fendorf, S. E. Surface reactions of chromium in soils and waters. *Geoderma* **1995**, *67* (1-2), 55-71.
(12) EPA, U. Chromium (VI)(CASRN 18540-29-9). *IRIS, US EPA ORD NCEA Integrated Risk Information System* **1998**, 1-33.
(13) Shahid, M.; Shamshad, S.; Rafiq, M.; Khalid, S.; Bibi, I.; Niazi, N. K.; Dumat, C.; Rashid, M. I. Chromium speciation, bioavailability, uptake, toxicity and detoxification in soil-plant system: A review. *Chemosphere* **2017**, *178*, 513-533.
(14) Rai, D.; Eary, L.; Zachara, J. M. Environmental chemistry of chromium. *Science of the total environment* **1989**, *86* (1-2), 15-23.
(15) Ostrowski, S. R.; Wilbur, S.; Chou, C.-H. S. J.; Pohl, H. R.; Stevens, Y.-W.; Allred, P. M.; Roney, N.; Fay, M.; Tylenda, C. A. Agency for Toxic Substances and Disease Registry's 1997 priority list of hazardous substances. Latent effects—carcinogenesis, neurotoxicology, and developmental deficits in humans and animals. *Toxicology and Industrial Health* **1999**, *15* (7), 602-644.
(16) Friess, S. L. Carcinogenic risk assessment criteria associated with inhalation of airborne particulates containing chromium (VI/III). *Science of the total environment* **1989**, *86* (1-2), 109-112.
Fehir, R. *Chemicals Evaluated for Carcinogenic Potential by the Office of Pesticide Programs* United States Environmental Protection Agency, United States Environmental Protection Agency, 2022.
(17) Organization, W. H. *Chromium in Drinking-water*; World Health Organization, 2020.
(18) Grace, M. R.; Spiccia, L. Early stages of the hydrolysis of chromium (III) in aqueous solution—VII. Kinetics of dimerization of deprotonated forms of doubly bridged dimer. *Polyhedron* **1991**, *10* (20-21), 2389-2397.
(19) James, B. R.; Bartlett, R. J. *Behavior of chromium in soils. VI. Interactions between oxidation-reduction and organic complexation*; Wiley Online Library, 1983.
(20) Bakshi, A.; Panigrahi, A. K. Chromium contamination in soil and its bioremediation: An overview. *Advances in Bioremediation and Phytoremediation for Sustainable Soil Management: Principles, Monitoring and Remediation* **2022**, 229-248.
(21) Ao, M.; Chen, X.; Deng, T.; Sun, S.; Tang, Y.; Morel, J. L.; Qiu, R.; Wang, S. Chromium biogeochemical behaviour in soil-plant systems and remediation strategies: A critical review. *Journal of Hazardous Materials* **2022**, *424*, 127233.

(22) Rai, D.; Sass, B. M.; Moore, D. A. Chromium (III) hydrolysis constants and solubility of chromium (III) hydroxide. *Inorganic Chemistry* **1987**, *26* (3), 345-349.
(23) Cotton, F. A.; Wilkinson, G.; Murillo, C. A.; Bochmann, M. *Advanced inorganic chemistry*; John Wiley & Sons, 1999.
(24) Moeller, T. Inorganic chemistry: a modern introduction. *(No Title)* **1982**.
(25) Haas, H. Fungal siderophore metabolism with a focus on Aspergillus fumigatus. *Natural product reports* **2014**, *31* (10), 1266-1276.
(26) Duckworth, O. W.; Akafia, M. M.; Andrews, M. Y.; Bargar, J. R. Siderophore-promoted dissolution of chromium from hydroxide minerals. *Environmental Science: Processes & Impacts* **2014**, *16* (6), 1348-1359.
(27) El-Shahawi, M. Chromium (III) complexes of naturally occurring ligands. *Spectrochimica Acta Part A: Molecular and Biomolecular Spectroscopy* **1995**, *51* (2), 161-170.
(28) Carbonaro, R. F.; Gray, B. N.; Whitehead, C. F.; Stone, A. T. Carboxylate-containing chelating agent interactions with amorphous chromium hydroxide: adsorption and dissolution. *Geochimica et Cosmochimica Acta* **2008**, *72* (13), 3241-3257.
(29) García Rodenas, L. A.; Iglesias, A. M.; Weisz, A. D.; Morando, P. J.; Blesa, M. A. Surface complexation description of the dissolution of chromium (III) hydrous oxides by oxalic acid. *Inorganic Chemistry* **1997**, *36* (27), 6423-6430.
(30) Saad, E. M.; Wang, X.; Planavsky, N. J.; Reinhard, C. T.; Tang, Y. Redox-independent chromium isotope fractionation induced by ligand-promoted dissolution. *nature communications* **2017**, *8* (1), 1590.
(31) Kim, S.; Chen, J.; Cheng, T.; Gindulyte, A.; He, J.; He, S.; Li, Q.; Shoemaker, B. A.; Thiessen, P. A.; Yu, B.; et al. PubChem 2023 update. *Nucleic Acids Research* **2022**, *51* (D1), D1373-D1380. DOI: 10.1093/nar/gkac956 (acccessed 2/6/2024).
(32) Tumolo, M.; Ancona, V.; De Paola, D.; Losacco, D.; Campanale, C.; Massarelli, C.; Uricchio, V. F. Chromium pollution in European water, sources, health risk, and remediation strategies: An overview. *International journal of environmental research and public health* **2020**, *17* (15), 5438.
(33) Zulfiqar, U.; Haider, F. U.; Ahmad, M.; Hussain, S.; Maqsood, M. F.; Ishfaq, M.; Shahzad, B.; Waqas, M. M.; Ali, B.; Tayyab, M. N. Chromium toxicity, speciation, and remediation strategies in soil-plant interface: A critical review. *Frontiers in Plant Science* **2023**, *13*, 1081624.
(34) Oliver, M. Soil and human health: a review. *European Journal of soil science* **1997**, *48* (4), 573-592.
(35) Ahmed, F.; Hossain, M. S.; MOHAMMAD, A. A.; Akbor, M. A.; AMINUL, A. M. Public health risk assessment of chromium intake from vegetable grown in the wastewater irrigated site in Bangladesh. **2016**.
(36) Zeng, F.; Ali, S.; Zhang, H.; Ouyang, Y.; Qiu, B.; Wu, F.; Zhang, G. The influence of pH and organic matter content in paddy soil on heavy metal availability and their uptake by rice plants. *Environmental pollution* **2011**, *159* (1), 84-91.
(37) Sahoo, H. B. Geology, Mining and Environment with an Overview of Sukinda Chromite Mines. *Journal of Earth and Environmental Sciences* **2017**. DOI: 10.29011/JEES-125. 100025.
(38) Mishra, S. R.; Pradhan, R. P.; Prusty, B. A. K.; Sahu, S. K. Meteorology drives ambient air quality in a valley: a case of Sukinda chromite mine, one among the ten most polluted areas in the world. *Environmental Monitoring and Assessment* **2016**, *188*, 1-17.
(39) Wang, M.; Chen, S.; Shi, H.; Liu, Y. Redox dependence of manganese controls cadmium isotope fractionation in a paddy soil-rice system under unsteady pe+ pH conditions. *Science of The Total Environment* **2022**, *806*, 150675.
(40) Hasan, M.; Kausar, D.; Akhter, G.; Shah, M. H. Evaluation of the mobility and pollution index of selected essential/toxic metals in paddy soil by sequential extraction method. *Ecotoxicology and environmental safety* **2018**, *147*, 283-291.
(41) Zhu, X.; Wang, K.; Yan, H.; Liu, C.; Zhu, X.; Chen, B. Microfluidics as an emerging platform for exploring soil environmental processes: a critical review. *Environmental Science & Technology* **2022**, *56* (2), 711-731.
(42) Wang, Y.; Soga, K.; Dejong, J. T.; Kabla, A. J. A microfluidic chip and its use in characterising the particle-scale behaviour of microbial-induced calcium carbonate precipitation (MICP). *Géotechnique* **2019**, *69* (12), 1086-1094.

(43) Borók, A.; Laboda, K.; Bonyár, A. PDMS bonding technologies for microfluidic applications: A review. *Biosensors* **2021**, *11* (8), 292.
(44) *Matlab*; 2012. https://de.mathworks.com/products/matlab.html (accessed 11.10.2023).
(45) *Microsoft Excel.*; 2018. https://office.microsoft.com/excel (accessed 11.10.2023).
(46) Nanda, S. P.; Panda, B. P.; Pradhan, A. Mining activities influencing the nutritional status of soil and water near a chromite mining site of Odisha, India. *Environmental Quality Management* **2022**, *32* (2), 151-159. DOI: 10.1002/tqem.21931.
(47) Dixit S, M. P., Muthukumar M, Reddy KM, Padhee AK and Mishra A. *Mapping the nutrient status of Odisha's soils.*; International Crops Research Institute for the Semi-Arid Tropics (ICRISAT) and Department of Agriculture, Government of Odisha, 2020.
(48) Tamaru, S.; Yabuta, S.; Goto, K.; Khanthavong, P.; Sakagami, J.-I. Oxygen consumption and transportation in rice roots are highly dependent on leaf area and root dry weight ratio. *Rhizosphere* **2023**, *25*, 100644.
(49) Babu, V. Soil organic carbon mapping and estimation of stock in rice soils of India. In *Proceedings of the Global Symposium on Soil Organic Carbon 2017, Rome, Italy, 21-23 March, 2017*, 2017; Food and Agriculture Organization of the United Nations (FAO): pp 32-34.
(50) Giannini, V.; Raimondi, G.; Toffanin, A.; Maucieri, C.; Borin, M. Agronomic management strategies to increase soil organic carbon in the short-term: evidence from on-farm experimentation in the Veneto region. *Plant and Soil* **2023**, 1-14.
(51) Liu, Y.; Ge, T.; van Groenigen, K. J.; Yang, Y.; Wang, P.; Cheng, K.; Zhu, Z.; Wang, J.; Li, Y.; Guggenberger, G. Rice paddy soils are a quantitatively important carbon store according to a global synthesis. *Communications Earth & Environment* **2021**, *2* (1), 154.
(52) Sadej, W.; Przekwas, K. Fluctuations of nitrogen levels in soil profile under conditions of a long-term fertilization experiment. *Plant Soil and Environment* **2008**, *54* (5), 197.
(53) Kudeyarova, A. Y. Aluminium phosphates as products of transformations of fertilizer phosphorus in an acid soil. *Geoderma* **1981**, *26* (3), 195-201.
(54) Mandal, B. K.; Vankayala, R.; Uday Kumar, L. Speciation of chromium in soil and sludge in the surrounding tannery region, Ranipet, Tamil Nadu. *International Scholarly Research Notices* **2011**, *2011*.
(55) Du Laing, G. Redox metal processes and controls in estuaries. *Wolanski E, McLusky DS. Treatise on estuarine and coastal science. Ed. Waltham: Academic Press. Publisher: Elsevier* **2011**, 115-141.
(56) Vollprecht, D.; Riegler, C.; Ahr, F.; Stuhlpfarrer, S.; Wellacher, M. Sequential chemical extraction and mineralogical bonding of metals from Styrian soils. *International journal of environmental science and technology* **2020**, *17*, 3663-3676.
(57) MINES, I. B. O. Indian Minerals Yearbook 2016. *Gov. India Minist. Mines Nagpur* **2018**, *13*, 1-17.
(58) Gabriel, K.; Salifoglou, A. A chromium (iii)-citrate complex from aqueous solutions. *Journal of Agroalimentary Processes and Technologies* **2005**, *11*, 57-60.
(59) Schmuck, C. *Chemie für Mediziner*; Pearson Deutschland GmbH, 2008.
(60) Brezonik, P.; Arnold, W. *Water chemistry: an introduction to the chemistry of natural and engineered aquatic systems*; OUP USA, 2011.
(61) Worch, E. *Hydrochemistry: basic concepts and exercises*; Walter de Gruyter GmbH & Co KG, 2023.
(62) Wood, J. K.; Black, V. K. XVI.—Amphoteric metallic hydroxides. Part III. Chromium hydroxide. *Journal of the Chemical Society, Transactions* **1916**, *109*, 164-171.
(63) Stewart, A. G.; Hudson-Edwards, K. A.; Dubbin, W. E. Effect of desferrioxamine B and Suwannee River fulvic acid on Fe (III) release and Cr (III) desorption from goethite. *Geochimica et Cosmochimica Acta* **2016**, *178*, 62-75.
(64) Kraemer, D.; Frei, R.; Viehmann, S.; Bau, M. Mobilization and isotope fractionation of chromium during water-rock interaction in presence of siderophores. *Applied Geochemistry* **2019**, *102*, 44-54.
(65) Thomas, G. W. Soil pH and soil acidity. *Methods of soil analysis: part 3 chemical methods* **1996**, *5*, 475-490.
(66) Kicińska, A.; Pomykała, R.; Izquierdo-Diaz, M. Changes in soil pH and mobility of heavy metals in contaminated soils. *European Journal of Soil Science* **2022**, *73* (1), e13203.

(67) Husson, O. Redox potential (Eh) and pH as drivers of soil/plant/microorganism systems: a transdisciplinary overview pointing to integrative opportunities for agronomy. *Plant and Soil* **2013**, *362*, 389-417.
(68) Xiao, W.; Ye, X.; Zhu, Z.; Zhang, Q.; Zhao, S.; Chen, D.; Gao, N.; Hu, J. Continuous flooding stimulates root iron plaque formation and reduces chromium accumulation in rice (Oryza sativa L.). *Science of the Total Environment* **2021**, *788*, 147786.
(69) Oshunsanya, S. *Soil pH for nutrient availability and crop performance*; BoD–Books on Demand, 2019.
(70) Hartemink, A. E.; Barrow, N. Soil pH-nutrient relationships: the diagram. *Plant and Soil* **2023**, *486* (1-2), 209-215.
(71) Zhang, Y.-Y.; Wu, W.; Liu, H. Factors affecting variations of soil pH in different horizons in hilly regions. *Plos one* **2019**, *14* (6), e0218563.
(72) Wang, X.; Tam, N. F.-Y.; He, H.; Ye, Z. The role of root anatomy, organic acids and iron plaque on mercury accumulation in rice. *Plant and soil* **2015**, *394*, 301-313.
(73) Colmer, T.; Cox, M.; Voesenek, L. Root aeration in rice (Oryza sativa): evaluation of oxygen, carbon dioxide, and ethylene as possible regulators of root acclimatizations. *New Phytologist* **2006**, *170* (4), 767-778.
(74) Hausladen, D. M.; Fendorf, S. Hexavalent chromium generation within naturally structured soils and sediments. *Environmental science & technology* **2017**, *51* (4), 2058-2067.
(75) Jiang, W.; Cai, Q.; Xu, W.; Yang, M.; Cai, Y.; Dionysiou, D. D.; O'Shea, K. E. Cr (VI) adsorption and reduction by humic acid coated on magnetite. *Environmental science & technology* **2014**, *48* (14), 8078-8085.
(76) Namgung, S.; Kwon, M. J.; Qafoku, N. P.; Lee, G. Cr (OH) 3 (s) oxidation induced by surface catalyzed Mn (II) oxidation. *Environmental science & technology* **2014**, *48* (18), 10760-10768.
(77) Gorny, J.; Billon, G.; Noiriel, C.; Dumoulin, D.; Lesven, L.; Madé, B. Chromium behavior in aquatic environments: a review. *Environmental Reviews* **2016**, *24* (4), 503-516.
(78) Hai, J.; Liu, L.; Tan, W.; Hao, R.; Qiu, G. Catalytic oxidation and adsorption of Cr (III) on iron-manganese nodules under oxic conditions. *Journal of hazardous materials* **2020**, *390*, 122166.
(79) Saad, E. M.; Sun, J.; Chen, S.; Borkiewicz, O. J.; Zhu, M.; Duckworth, O. W.; Tang, Y. Siderophore and organic acid promoted dissolution and transformation of Cr (III)-Fe (III)-(oxy) hydroxides. *Environmental Science & Technology* **2017**, *51* (6), 3223-3232.
(80) Santawaja, P.; Kudo, S.; Tahara, A.; Asano, S.; Hayashi, J.-i. Dissolution of iron oxides highly loaded in oxalic acid aqueous solution for a potential application in iron-making. *isij international* **2022**, *62* (12), 2466-2475.
(81) Wang, Y.; Stone, A. T. Reaction of MnIII, IV (hydr) oxides with oxalic acid, glyoxylic acid, phosphonoformic acid, and structurally-related organic compounds. *Geochimica et Cosmochimica Acta* **2006**, *70* (17), 4477-4490.
(82) Andrade, E.; Miyazawa, M.; Pavan, M. A.; Oliveira, E. L. d. Effect of organic matter on manganese solubility. *Brazilian Archives of Biology and Technology* **2002**, *45*, 17-20.
(83) Dong, Z.; Wen, Z.; Zhao, F.; Kuhn, S.; Noël, T. Scale-up of micro-and milli-reactors: An overview of strategies, design principles and applications. *Chemical Engineering Science: X* **2021**, *10*, 100097.
(84) Bhattacharjee, A.; Khan, M.; Kleiman, M.; Hochbaum, A. I. Effects of growth surface topography on bacterial signaling in coculture biofilms. *ACS applied materials & interfaces* **2017**, *9* (22), 18531-18539.
(85) Bhattacharjee, A.; Qafoku, O.; Richardson, J. A.; Anderson, L. N.; Schwarz, K.; Bramer, L. M.; Lomas, G. X.; Orton, D. J.; Zhu, Z.; Engelhard, M. H. Fungal Mineral Weathering Mechanisms Revealed Through Direct Molecular Visualization. *bioRxiv* **2021**, 2021.2010. 2001.462718.
(86) Webster, N. A.; Loan, M. J.; Madsen, I. C.; Knott, R. B.; Kimpton, J. A. An investigation of the mechanisms of goethite, hematite and magnetite-seeded Al (OH) 3 precipitation from synthetic Bayer liquor. *Hydrometallurgy* **2011**, *109* (1-2), 72-79.
(87) Huang, C.-C.; Wu, M.-D.; Liang, D.; Yu, J.; Shih, P.-J.; Shih, W.-P. Fabrication and application of iron (III)-oxide nanoparticle/polydimethylsiloxane composite cone in microfluidic channels. *Journal of Nanomaterials* **2012**, *2012*, 8-8.

(88) Siddique, M. A. B.; Arif, R. B.; Khan, M. M. R. Digital image segmentation in matlab: A brief study on otsu's image thresholding. In *2018 international conference on innovation in engineering and technology (ICIET)*, 2018; IEEE: pp 1-5.
(89) Papassiopi, N.; Vaxevanidou, K.; Christou, C.; Karagianni, E.; Antipas, G. Synthesis, characterization and stability of Cr (III) and Fe (III) hydroxides. *Journal of hazardous materials* **2014**, *264*, 490-497.
(90) Alzahid, Y. A.; Mostaghimi, P.; Gerami, A.; Singh, A.; Privat, K.; Amirian, T.; Armstrong, R. T. Functionalisation of polydimethylsiloxane (PDMS)-microfluidic devices coated with rock minerals. *Scientific reports* **2018**, *8* (1), 15518.
(91) Ruiz-Garcia, M.; Stanberry, J.; Ribeiro, G. B.; Anagnostopoulos, V. Oxidative dissolution of Cr (OH) 3 and mixed Fe-Cr (III) phases by aqueous Mn (III)-pyrophosphate complex. *Journal of Environmental Sciences* **2024**, *139*, 105-113.
(92) Sunda, W.; Huntsman, S. Effect of pH, light, and temperature on Fe–EDTA chelation and Fe hydrolysis in seawater. *Marine Chemistry* **2003**, *84* (1-2), 35-47.
(93) Schindler, M.; Lussier, A. J.; Principe, E.; Mykytczuk, N. Dissolution mechanisms of chromitite: Understanding the release and fate of chromium in the environment. *American Mineralogist* **2018**, *103* (2), 271-283.
(94) Mishra, S.; Shanker, K.; Srivastava, M.; Srivastava, S.; Shrivastav, R.; Dass, S.; Prakash, S. A study on the uptake of trivalent and hexavalent chromium by paddy (Oryza sativa): possible chemical modifications in rhizosphere. *Agriculture, ecosystems & environment* **1997**, *62* (1), 53-58.
(95) Sharma, A.; Kapoor, D.; Wang, J.; Shahzad, B.; Kumar, V.; Bali, A. S.; Jasrotia, S.; Zheng, B.; Yuan, H.; Yan, D. Chromium bioaccumulation and its impacts on plants: an overview. *Plants* **2020**, *9* (1), 100.
(96) Prasad, S.; Yadav, K. K.; Kumar, S.; Gupta, N.; Cabral-Pinto, M. M.; Rezania, S.; Radwan, N.; Alam, J. Chromium contamination and effect on environmental health and its remediation: A sustainable approaches. *Journal of Environmental Management* **2021**, *285*, 112174.
(97) Costa, M.; Klein, C. B. Toxicity and carcinogenicity of chromium compounds in humans. *Critical reviews in toxicology* **2006**, *36* (2), 155-163.
(98) Alvarez, C. C.; Gómez, M. E. B.; Zavala, A. H. Hexavalent chromium: Regulation and health effects. *Journal of Trace Elements in Medicine and Biology* **2021**, *65*, 126729.
(99) Laboratory, R. *Ronald lab rice growing protocol*. 2020. https://kitbase.ucdavis.edu/pdf/rice-growing-protocol-Jan2020.pdf (accessed.

APPENDIX

A. Aqua Regia Solution Preparation according to CHEM-LM-SOP-03 (University of Toronto)

Assemble ingredients inside this fume hood:

- Concentrated hydrochloric acid
- Concentrated nitric acid

Choose the right type and size of container. Slowly add the nitric acid to the hydrochloric acid (never the other way around) to form a 3:1 ratio solution of three parts hydrochloric acid, and one-part nitric acid. Stirring with a stir bar and plate is recommended.

Note: The resulting solution appears at first colourless and clear but will quickly acquire a transparent orange colour upon mixing.
This reaction is very exothermic; the solution may bubble and heat up to temperatures in excess of 100°C. Allow for the solution to react for a few minutes and reach a high temperature before immersing glassware to be cleaned.
If glassware was previously immersed in aqua regia solution, ensure that all traces of aqua regia have been removed through rinsing with distilled water.
Allow glassware to be immersed in aqua regia for five to ten minutes. Stirring or manual scrubbing is not required and highly discouraged.
Carefully remove the glassware from the aqua regia solution, and rinse thoroughly with distilled water (always working inside the fume hood).

B. Rice growing protocol according to "Ronald lab rice growing protocol (February, 2020)"

The Protocol was used as a guideline for the rice mesocosm experiment. It was obtained from the university of California, Davis Webpage [99].

1. Seed germination

Use a mortar and pestle to gently grind each rice seed to remove the husk before it germinates. For thirty minutes, soak dehusked seeds in 30% household bleach. Use sterile water to thoroughly rinse at least three times. Fill a Solo cup (Dart Solo SD5, and SDL58) with ½ MS media, 20 disinfected seeds, and adjust the pH to 5.8, add agar to 0.8%, autoclave the mixture for 15 minutes, and incubate for 7 days at 28°C under fluorescent light for 14 hours and 26°C under darkness.

2. Growing rice in tubs in the greenhouse

After a week in MS media, move the rice seedlings to a hydroponic system (for growth chamber) or to soil (for greenhouse growth) (see point 5). Sand soil mix (80% sand, 20% peat; Redi-Gro, Sacramento, CA; http://www.redi-gro.com/) should be filled into5" square pots up to one inch below the top rim. Put three seedlings in each pot; this will work well for most uses. After putting the pots in the 24" x 36" black tubs, fill the tubs with fertilized water (just below the soil's surface; don't overflow). Prepare concentrated stocks A and B (see below), mix 1:1, and dilute 200 times with reverse osmosis (RO) water to create the fertilizer water. To measure the electrical conductivity (EC), use an EC meter (HM Digital, AP-2). The final EC reading should be 800 -1000 uS/cm.

200X Concentrated fertilizer water			
Tank A, 10 gallons		Tank B, 10 gallons	
Components	Mass (g)	Components	Mass (g)
Calcium Nitrate	1076	Monopotassium Phosphate	666
Potassium Nitrate	800		
Iron EDDHA	189.2	Ammonium Sulfate	1330
Zinc EDTA	2.7	Magnesium Sulfate	1313
Copper EDTA	1.08	Potassium Sulfate	166
Manganese EDTA	29.2		
Sodium Molybdate	0.19		

3. Water, fertilizer, temperature, humidity, and light

Fill greenhouse tubs to the brim with fertilizer water every day. RO water can be added to plants after they have flowered. In a greenhouse, daytime temperatures range from 27–29°C, while nighttime temperatures are between 19.5-21.5°C. The range of relative humidity (RH) is 50–95%. Twenty fixtures of 1000w High Pressure Sodium light bulbs are used in the main greenhouse of Ronald Lab. In Davis, California, natural light is sufficient for rice cultivation from April to October 1. Every year on May 1st, the greenhouse staff turns off the lights, and on October 1st, they turn them back on. When outside light falls below 400W/square meter, the greenhouse staff will start supplementing with artificial lights on October 1st and run them from 6 am to 10 pm.

4. Pesticide spraying

Keep an eye out for pests like thrips, spider mites, and aphids in the greenhouse. Maybe a pesticide mist is required. Observe rules to ensure safe spraying.

5. Hydroponic Growth in growth chambers

Growing rice in a growth chamber using a hydroponic system is an alternate method.

Rice seedlings should be transplanted into 2" A-Ok Starter PlugsTM inside 10" by 20" flats that have been soaked in 1 X Hoagland Nutrient Solution after one week in MS media (see above). Transfer rice to a growth chamber that has 14 hours of fluorescent light at 26°C and 10 hours of darkness at 24°C with 85% relative humidity. Every two to three days, swap out the nutrient solution.

1000X-Hoagland Nutrient Solution	
NH_4NO_3	80 g
$NaH_2\ PO_4 \cdot 2H_2O$	93 g
K_2SO_4	52.4 g
$CaCl_2 \cdot 2H_2O$	44.2 g
$MgCl_2 \cdot 6H_2O$	122 g
FeEDTA	19 g
H_2BO_3	3.01 g
$MnSO_4 \cdot 5H_2O$	2.17 g
$CuSO_4 \cdot 5H_2O$	0.075 g
$ZnSO_4 \cdot 7H_2O$	0.2008 g
$Na_2MoO_4 \cdot 2H_2O$	0.024 g
pH	5.6-5.8

6. Seed harvesting and storage

Gather seeds in envelopes once they turn brown, which happens about a month after flowering.

Following harvest, dry the seeds in an oven set to 50°C for five to seven days. Then, store the seeds for short-term storage at 20°C or for long-term storage at 14°C with 14 percent relative humidity.

7. For seed increase and crosses

The best months to plant Kitaake rice in Davis, California, are January through August, for a good seed set. We can't keep our greenhouses warm enough during the winter for the best seed set, so rice planted between late August and early December produced fewer seeds. You must either isolate the same rice genotype by time or space, or bag the panicles just prior to flowering to prevent cross-pollination, in order to obtain true-to-type seeds.

After flowering, the glassine bag can be removed to obtain healthy (non-discolored) seeds. For optimal germination, seeds must be harvested at the ripe stage. Seeds harvested too soon or too late will not sprout properly. For crosses, use small sharp scissors to cut off the top of each spikelet in a panicle at a

slight angle. Then, use fine point forceps to remove the anthers from each spikelet, or vacuum in the early morning (before 9:00am) or late afternoon (after 5:00pm), when the panicle emerges from its sheath to the majority of its length. Remove the basal spikelets from the panicle (which are too young to cross) and the top spikelets (which may self-pollinate). Put a glassine bag over the panicle containing the pollen parent panicle and the panicle of fully emasculated spikelets. During flowering, gently tap (flick) the glassine bag every 30 minutes (11:00 am to 2:00 pm). In order to produce the most hybrid seeds, pollination should take place over the course of two to three days.

C. Standard solution preparation

All chemicals, solvents and buffers used were purchased at Sigma Aldrich and used without further purification except when mentioned specifically.

a. Pot experiment ligand standard solutions

i. Desferrioxamine B

For 0.1mM Desferrioxamine B (DFOB), the standard solution was prepared by adding Desferoxamine (Desferal 500mg, Novartis, Switzerland) to DI water.

ii. Oxalic acid

For 10mM oxalic acid, the standard solution was prepared by adding oxalic acid (90.03 g/mol) to DI water.

b. Microfluidic reactor experiment standard solutions

i. Chromium(III)-(oxy)hydroxides

Chromium(III)hydroxide ($Cr(OH)_3$), was prepared by adding a solution of ammonium hydroxide (NH_4OH) to a solution of chromium salt ($CrCl_3$). The pH was adjusted to pH 7 using NaOH.

ii. Manganese Pyrophosphate

For 100 µM Manganese Pyrophosphate (Mn-PP), the standard solution was prepared by adding a pyrophosphate solution to Mn(III)-acetate particles with a ratio of 20:1. The solutions were stirred vigorously under a N_2(g) environment for 24h and filtered prior to measurement. The Mn-PP solution has a light pink coloration at pH 8.

iii. Oxalic acid

For 0.1 M oxalic acid, the standard solution was prepared by the addition of oxalic acid (90.03 g/mol) to DI water. The pH was adjusted to 7 using NaOH and stabilized with 10mM Hepes Buffer.

iv. Ethylenediaminetetraacetic acid

For 0.1 M EDTA, the standard solution was prepared by the addition of Ethylenediaminetetraacetic acid (292.24 g/mol) to DI water. The pH was adjusted to 7 using NaOH and stabilized with 10mM Hepes Buffer.

D. Ferrozine assay – Spectrophotometric determination of Fe(II) and Fe(III)

Principle:

Dissolved ferrous iron, Fe^{2+}, reacts with ferrozine (Na_2-3-/2-pyridyl)-5-6-bis (4-phenylsulfonate)-1,2,3-triazine) and forms an intensively purple-coloured complex. This complex can be quantified spectrophotometrically at 562 nm using the plate reader or the cuvette photometer in S 106. The Fe(III) content is determined as difference between Fe(tot) and Fe(II). Therefore, the total Fe-content gets reduced using HAHCl (hydroxylamine hydrochloride). The absorption is linear in the range from 0-100 µM of Fe^{2+}. If higher concentrations can be expected, pre-dilutions are necessary. Usually, the Ferrozine assay is performed in 96-well plates using the plate reader.

Reagents:

- Hydroxylamine hydrochloride (HAHCl): 10% (w/v) in 1 M HCl. Wrap bottle in tinfoil and store in the dark at 4°C.
- Ferrozine: 0.1% (w/v) in 50% (w/v) ammonium acetate. Wrap bottle in tinfoil and store in the dark at 4°C.
- 1 M HCl
- $(NH_4)_2Fe(SO_4)_2$ x $6H_2O$ in 1 M HCl in the expected Fe concentration range (standards usually range from 0-1000 µM Fe^{2+} (before dilution, see procedure!). Store at 4°C.
- Prepare all solutions in measuring flasks, do not use beaker or Schott bottles etc.!

Procedure (for measurements using the plate reader):

Each sample is measured in an instrumental triplicate.

Total Fe:

1) add 80 µl HAHCl per well

2) add 20 µl sample/standard per well and incubate for 30 minutes in the dark

3) add 100 µl ferrozine per well and incubate for 5 minutes in the dark

4) measure absorbance at 562 nm

Fe^{2+}:

1) add 80 µl 1M HCl per well

2) add 20 µl sample/standard per well

3) add 100µl ferrozine per well and incubate for 5 minutes in the dark

4) measure absorbance at 562 nm.

Plate with 200 µl DI-water per well is used as a blank and must be measured first!

For small concentrations you might consider using the 50 µl (sample):50 µl (HCl/HAHCl):100 µl (ferrozine solution) approach.

Calibration curve and procedure:

You need two calibration curves. One for Fe(II) with HCl and a second one for Fe(tot) with HAHCl. Plot your data and calculate the regression curve for your standards. Based on this equation you can calculate the concentrations of Fe in your sample. You can store your standards up to two months in the fridge. A new calibration should be performed with each measurement.

Concluding remarks:

Fe(II) oxidizes very fast in an abiotic reaction to Fe(III) under oxic conditions at neutral pH. Acidified using 1 M HCl your sample can be stored in the fridge without oxidation of Fe(II) to Fe(III). Do not use 6 M HCl for stabilization as it was shown that Fe(II) gets re-oxidized (Porsch & Kappler 2011). If there is nitrite present in your sample the above described procedure has to be changed, as nitrite will interfere with Fe(II) at acidic pH.

E. MATLAB Image analysis script

```
% Assign and enter working directory
WD = [RD ExperimentName '/' FolderPath '/' Subfolder];
cd(WD);

% Acquire names of all images, store in structure
ims = dir('*.tif');
ims = ims(~startsWith({ims.name},'._'));
ImageName = {ims.name};

% Create output folder for final images
mkdir Final
Final = [WD '/Final'];

%% Load images
Image = imread(ImageName{1,1});
f1 = figure(1);
imshow(Image);

%% Crop/rotate/binarize/etc images
imcrop(Image);

%% Fix cropped image
CroppedImage = imcrop(Image, [9726.5 1211.5 9043 6189]);
f2 = figure(2);
imshow(CroppedImage);
```

```
%% Binarize images
GrayImage = rgb2gray(CroppedImage);
f3 = figure(3);
imshow(GrayImage);

%%
BW = imbinarize(GrayImage);
f4 = figure(4);
imshow(BW);

%%
BW2 = imbinarize(GrayImage, 'adaptive', 'Sensitivity', 0.85);
f5 = figure(5);
imshow(BW2);

%%
% To use regionprops(), first label your image
InverseImage = imcomplement(BW2);
LabMask = bwlabel(InverseImage);
rgbLabel = label2rgb(LabMask, @prism, [0.5, 0.5, 0.5]);
f6 = figure(6);
imshow(rgbLabel);
stats = regionprops('table', LabMask, 'Area', 'Perimeter');

 %% Filtering by area
BWFiltered = bwareafilt(InverseImage, [1 2000000]);
%BWFiltered = bwareafilt(BW2, [1 7000]);
f7 = figure(7);
imshow(BWFiltered);

%% Sum up all mineral pixels in image
% Assign variable here
FinalImMask = BWFiltered;
MineralSum = sum(FinalImMask, 'all');
ImageArea = size(FinalImMask, 1) * size(FinalImMask, 2);
PercMineral = MineralSum / ImageArea * 100

%% Save images
cd(Final);
saveas(f5, 'Filtered_Image.png'); % Can be any image format (.png, .jpg, .tif)
saveas(f5, 'Filtered_Image.fig'); % Matlab figure format

saveas(f6, 'Labeled_Image.png'); % Can be any image format (.png, .jpg, .tif)
saveas(f6, 'Labeled_Image.fig'); % Matlab figure format

saveas(f7, 'Filtered_Image.png'); % Can be any image format (.png, .jpg, .tif)
saveas(f7, 'Filtered_Image.fig'); % Matlab figure format

%% Save variables
save('Mineral_Statistics.mat', 'stats');
% load('Mineral_Statistics.mat');
```

Acknowledgements

I want to thank Stephan Krämer for the opportunity to work on this master's thesis in his lab. Furthermore, I especially want to express my gratitude to him for making it possible to conduct one part of the project at the University of California in Davis.

There, I had the pleasure of acquiring knowledge in a very exciting topic, microfluidic devices and image analysis. This would not have been possible without the Members of the Civil and Environmental Engineering department. A big thank you to Jasquelin Peña for letting me be part of this group and to Ella Fadely for guiding me with the project. Additionally, I would like to say thanks to Libby, Gaitan and Lim for all the help and openness I received.

Also, I want to thank Naresh Kumar for bridging the gap between the Research conducted on-site in India and the Scientists working in Vienna. This was very helpful!

A big thank you goes to all the members and lab technicians (Herwig, Kyle, and Sofie) for the amazing work environment, openness to questions, technical advice, and many shared lunches.

Lastly, I want to thank Johannes and Wenhao, who are also working on the Chromium project, for their support during my master's project.